Recurrent Neural Network-based Digital Pre-Distortion for Wideband Radio Frequency Power Amplifiers

Master Thesis

Yizhuo Wu

Delft University of Technology

TU Delft

Recurrent Neural Network-based Digital Pre-Distortion for Wideband Radio Frequency Power Amplifiers

by

Yizhuo Wu

Student Name	Student Number
Yizhuo Wu	5473241

Instructor:	Dr. Chang Gao
Institution:	Delft University of Technology
Project Duration:	09, 2022 - 08, 2023

TU Delft

Acknowledgments

After two years at TU Delft, I am about to graduate from the master's program and continue pursuing a doctoral degree at the same institution. TU Delft has completely transformed my perception of education, capturing my interest with its well-designed curriculum and course content. The systematic approach to education and research, along with direct and efficient discussions and practical experiences, are the education styles that I admire the most.

Here, I would like to express my heartfelt gratitude to my supervisor, Dr. Chang Gao. I am incredibly fortunate to have chosen him as my master's thesis supervisor during the year he arrived at TU Delft. His research focus is exactly the direction I am most eager to be involved in. His enthusiasm for work, extensive professional knowledge, and infinite patience have guided me through various challenges in my thesis project. I still remember being amazed by his ability to quickly identify potential problems in my work, even after extended periods of sleepless work. Additionally, he has provided me with valuable advice on project management, time planning, and other strategies to enhance research efficiency, which has benefited not only my master's thesis but also my overall academic experience.

I would also like to express my gratitude to our research team, ELCA. Professor Leo de Vreede helped with instruments throughout the entire experimental process. Ing. Mr. Marco Pelk and Dr. Morteza Alavi assisted me in resolving issues encountered during my experiments. Mr. Gagan Singh devoted a significant amount of time to helping me with testing and patiently answering my questions.

In addition, I am thankful for my best friends. Ms.Ruohan Zhong accompanied me through every moment of low spirits. Journeying alongside her has been one of the driving forces behind my pursuit of a doctoral degree. I extend my appreciation to my office mates, Mr. Lianbo Liu and Mr. Tzonglin Chua, for their continuous patience and assistance.

I would also like to express my gratitude to my family. My dear mother has been my pillar of strength, providing me with the courage to face challenges throughout my life. I am thankful to my father for understanding my decision to study abroad and for offering his unwavering support. I appreciate my grandparents for nurturing and raising me.

Finally, I give an appreciation to myself, as a woman, for persevering every step of the way.

Yizhuo Wu
Delft, August 2023

Abstract

With the advancement of 5G/6G radio networks, the demand for high-performance power amplifiers (PAs) with clean spectra and compact constellations has increased significantly. To address these challenges, Artificial Intelligence (AI)-based digital predistortion (DPD) has emerged as a promising approach to linearize radio-frequency (RF) PAs. However, existing state-of-the-art AI-based architectures rely on computationally expensive online feature extraction to achieve satisfying linearization performance, resulting in complicated algorithm data paths and difficulty in energy-efficient hardware implementation. This thesis proposes a new deep recurrent neural network (RNN)-based DPD architecture, called Skip Gated Recurrent Unit (SGRU), with precise offline baseband signal feature extraction to bypass the need for complex online feature extraction while still maintain high linearization performance. The proposed RNN architecture employs the end-to-end (E2E) learning framework to implement an efficient DPD model. By combining the offline feature extraction and E2E framework, we achieved a more streamlined and faster training method for wideband RF power amplifier (PA) DPD. With a simplified neural network architecture and fewer parameters, our approach utilizes 394 parameters to achieve adjacent channel power ratio (ACPR) (lower/upper) of -45.16/-44.31 dBc for 100 MHz orthogonal frequency division multiplexing (OFDM) signal, ACPR (lower/upper) of -38.44/-42.09 dBc for 200 MHz OFDM signal. Compared to previous state-of-art phase gated just-another-network (PG-JANET) [1] and decomposed vector rotation just-another-network (DVR-JANET) [2], our approach has better ACPR and error vector magnitude (EVM) performance with parameters around 400. Compared to vector decomposition long-short term memory (VDLSTM) [3], our approach achieves a better lower/upper band balance.

Contents

Acronyms

ACPR adjacent channel power ratio ii
ADC Analog-to-Digital converter 18
AI Artificial Intelligence ii
AM Amplitude Modulation 4
ANNs Artificial Neural Networks 8
ARVTDNN augmented real-valued time-delay neural network vii
AVDTDNN Augmented Vector decomposition time-delay neural network ix
CNN Convolutional Neural Network 16
CNNs Convolutional Neural Networks 7
DAC Digital-to-Analog converter 18
DLA direct learning architecture vii
DNNs Deep Neural Networks 7
DNN Deep Neural Network ix
DPD digital predistortion ii
DVR decomposed vector rotation 15
DVR-JANET decomposed vector rotation just-another-network ii
E2E end-to-end ii
EVM error vector magnitude ii
FRNN Full recurrent neural network 11
GMP generalized memory polynomial ix
GRU gated recurrent unit 11
IGIRNN instant gated implicit recurrent neural network ix
IFFT Inverse Fast Fourier Transform 22
ILA indirect learning architecture vii
ILC iterative learning control 2
JANET just-another-network 15
LSTM long-short term memory ix
MLP Multilayer Perception 7
MP Memory polynomial 18
MSE mean square error 13
NMSE normalized mean-square error 2
NN Neural Network 1
NNs Neural Networks 1

List of Figures

List of Tables

1 Introduction

RF PAs face the problem of generating in-band distortion and out-of-band spurious emissions due to operating in the saturation region. To mitigate this issue, the DPD module is incorporated into the wireless transmitter system's baseband digital signal processor. The core concept of DPD is to identify an inverse PA function to compensate for the nonlinearity of PA. In traditional wireless systems, DPD has been approved as a better method to improve linearity than feedforward and "linear amplification with nonlinear components" methods [4]. However, in next-generation (5G/6G) wireless systems, the requirement of high-performance DPD has been increased because of the wideband spectrum. Wideband spectrum with high-order modulation limits PA at serious back-off and causes severe nonlinearity.

Before Neural Networks (NNs), GMP is regarded as a state-of-the-art model to implement DPD and is currently still the fact standard in the industry. GMP was invented based on Volterra series methods and other special cases, such as parallel Hammerstein [5]. Even if GMP showed good performance in prior works, their ability to catch the non-linearity faces more and more challenges when operating at high peak-to-average power ratio (PAPR) and with large bandwidth signals [6]. To overcome the model capability challenge, NNs are gradually adopted to implement non-linear DPD due to their ability to fit arbitrary nonlinear functions.

This thesis focuses on creating a high-performance AI-based DPD framework for next-generation RF PA. The new framework contains an E2E learning architecture and a SGRU DPD model. Previous learning architecture ILA holds the assumption that RF PAs are commuted, which is not practical. The proposed learning architecture should waive this assumption. Meanwhile, it should decrease the computational cost. The proposed DPD Neural Network (NN) model should have competitive calculation complexity when operating wideband signal on RF PA

1.1. Problem Statement and Research Questions

1.1.1. Problem Statement

Based on the literature review of prior DPD works, the challenges and problems faced by AI-based DPD tasks are explored and concluded in this subsection.

Firstly, there was no unitary standard to compare the performance of different DPD methods, given that most prior works used different PAs. Moreover, PA non-linear characteristics, learning architecture, and the experimental setup could also be factors that lead to better linearization performance of a DPD method besides the algorithmic model. Studying these factors helps to find more insights for the evaluation of different DPD methods.

Secondly, the traditional learning architecture of DPD has a complex procedure or has impractical assumptions, such as the PA is commuted while finding the ideal input. It is worth finding a learning architecture that can bypass these two problems at the same time.

Thirdly, the number of parameters and the computational complexity of prior DPD methods are not friendly to cost-efficient hardware design. Although the latest works generate better ACPR and normalized mean-square error (NMSE) than before, their performance gain still relies on substantially increasing the number of parameters and computational complexity. The complicated online feature extraction layer can increase the training time of the model and decrease the operations that can be parallel, making it difficult to realize an energy-efficient hardware implementation of the DPD method. Therefore, it is essential to try to decrease the complexity of NN DPD architectures while maintaining satisfactory performance.

1.1.2. Research Questions

This thesis mainly focuses on the following questions.

1. What are the variables that must be identified in the work of DPD? That is, in the test of the DPD performance, what are the variables that may decisively affect the test result?

2. Can a simpler and more practical learning architecture be found with the help of neural networks in modeling the time-domain behaviors of PAs?

3. Instead of capturing important features of DPD through complex input layers, Could we find a new NN architecture to simplify the computational complexity of AI-based DPD and improve its hardware friendliness?

1.2. Thesis Contributions

The main contribution of this thesis is summarized below.

1. We introduce a new E2E learning architecture that waives the assumption that PA is commuted and eliminates the complex calculation in iterative learning control (ILC). This new E2E learning architecture firstly digitizes RF PA by a NN model. Then cascade DPD NN and frozen digital PA NN to train DPD through backpropagation.

2. We proposed a NN-based DPD architecture, called SGRU, that demonstrates better NMSE and ACPR performance than previous state-of-art architecture when linearizing 100 MHz and 200 MHz OFDM signal on specific Class-AB (CGH40006s-AMP1) and Doherty (Ampleon C5H38110AX) PAs. From analysis, this architecture also decreases the computation complexity.

1.3. Thesis Outline

The rest of the thesis is organized as follows.

Chapter 2:Back Ground and Related Works: This chapter first introduces the background of DPD in Section 2.1 and 2.2. Then cites GMP as a baseline model in Section 2.3. In the third Section 2.4, different NNs architecture shows milestone techniques in NN-based DPD. Decisive variables of AI-based DPD are discussed at the end of section 2.7.

Chapter 3:Methods: This chapter introduces the proposed E2E learning architecture in the first Section 3.1. Secondly, Section 3.2 shows motivations and details of the SGRU architecture. The third section 3.3 explains how we chose four features for the proposed architecture.

Chapter 4 Experimental Setup and Results: This chapter introduces the experimental settings and results of different validation platforms. Section 4.1 introduces the early validation on the simulated platform. RF WebLab online validation platform results in Section 4.2 offers results that can be rebuilt and compared on an open-source platform. Section 4.3 and Section 4.4 validate the performance of the proposed architecture on Class-AB and Doherty

test boards with commercial instruments, respectively. Finally, Section 4.5 discussed the special data preprocessing step in the RFWebLab experiment, the reason analysis for different results from previous work, and the computational complexity analysis.

Chapter 5: Conclusion, Limitation, and Outlook: This Chapter concludes the advantages and disadvantages of the proposed architecture and framework. At the end of this thesis, we look forward to the possible improvement of our work, the new topic we found in the related systems, and possible cooperation with PA design.

2

Background and Related Work

In the beginning, this chapter explains the requirement of linearity in RF PA in Section 2.1 and introduces the DPD concept in wireless systems in Section 2.2. Subsequently, we will present GMP as a baseline model, a performance comparison standard for this chapter in Section 2.3. The following three sections 2.4, 2.5 and 2.6 introduce the design of the NN architecture, the choice of learning architecture, and the different validation experimental platforms, respectively. These three sections help to gain insight into the DPD design and implementation process. Finally, section 2.7 includes comparing performance and arguments of three implementation steps. A summary of related work is given at the end.

2.1. Nonlinearity in RF Power Amplifier

RF PA operates near the saturation region to gain efficient signal transmission, but this comes at the cost of unwanted growth of the spectrum out of the allocated channel. This unwanted growth of the spectrum reflects the nonlinear behavior introduced near the transferring performance. PAs' nonlinear behavior generates harmonic and intermodulation distortion by operating the input signal. While harmonic distortion can be mitigated using post-PA filtering, intermodulation distortion requires the application of linearization techniques such as DPD.

To accurately model distortion, DPD techniques must take into account various contributing factors. On the one hand, the active components in the system have a dynamic transfer function. The complex gain of PAs can't be a stable, unique value for different inputs in practice. The variance of gain introduces Amplitude Modulation (AM) non-linearity and Phase modulation (PM) non-linearity simultaneously. These two modulation non-linearities are often reflected by AM-AM and AM-PM curves.

On the other hand, the system's previous state impacts its current behavior as a result of the presence of active components. For example, the thermal effect that generates heat affects the characteristic of PA, leading to what is commonly known as the memory effect.

Further insights into the RF PA nonlinearity analysis that can contribute to the design of the DPD model will be shown in the section 3.2.1.

2.2. DPD and Its Metrics in Wireless Systems

The fundamental idea behind DPD is to determine an inverse function of PA transfer function, which serves to compensate for the non-linear behavior exhibited by the PA as depicted in Figure 2.1. Based on this simple concept, the challenges of DPD revolve around identifying an appropriate model, an effective learning architecture, and low-cost hardware for the realization of high-performance DPD.

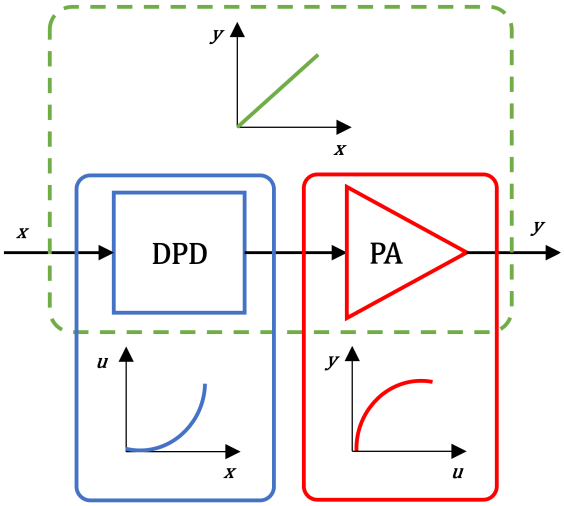

Figure 2.1: Concept of DPD.

When evaluating the effectiveness of such techniques, there are four common metrics, NMSE, ACPR, EVM, and the number of parameters, to assess the performance of AI-based DPD.

The first, NMSE, reflects the precision of the AI model. When all previous works use $I(n)$ and $Q(n)$ as target output, NMSE calculation function is shown in Function 2.1. N is the number of test data samples.

$$NMSE = 10 \times log10(\frac{\frac{1}{N}\sum_{n=1}^{N}((\hat{I}_{out,n} - I_{out,n})^2 + (\hat{Q}_{out,n} - Q_{out,n})^2)}{\frac{1}{N}\sum_{n=1}^{N}((I_{out,n})^2 + (Q_{out,n})^2)}) \tag{2.1}$$

Under the same learning architecture and the same NMSE calculation, ACPR is hoped to have the same trend as NMSE. However, different works always use different methods to obtain the ideal input signal, affecting the PA modeling accuracy. For commercial measurement instruments, the ACPR shows a discrepancy between the radio frequency signal and the collected baseband signal. ACPR is regarded as one of the most important metrics of RF PA DPD. The definition of ACPR is $10 \times log10(\frac{Adjacent\,Channel\,Power}{Main\,Channel\,Power})$.

Third, EVM can evaluate the performance of digital transmitters. This metric holds significance to demodulate the signal and transmit information accurately. Take 4-Quadrature amplitude modulation (QAM) in Figure 2.2 for example, the EVM is defined as the root mean square error average amplitude of error vector normalized the ideal input amplitude.

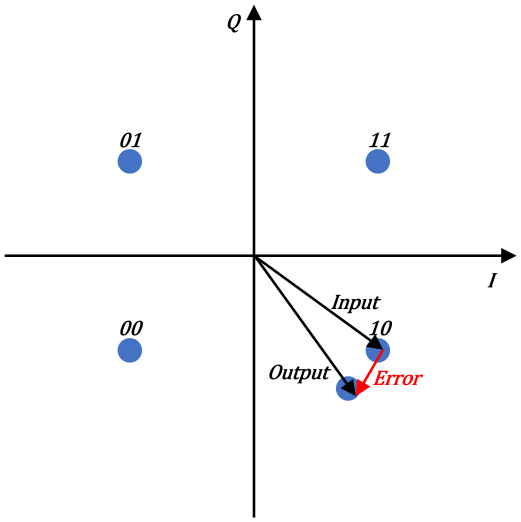

Figure 2.2: Constellation for 4-QAM and EVM.

Finally, the computational complexity can seriously impact the hardware cost. To accurately reflect the calculation complexity, it's essential to consider the operation details and hardware implementation performance. Although the number of parameters can partially serve as a representative metric, it may not precisely reflect computational complexity.

2.3. Baseline: Generalized Memory Polynomial Model

NN-based DPD model widely use GMP as performance baseline. Before adopting the deep learning technique, GMP was a state-of-art model because of its good performance compared with earlier models, such as adaptive linearizer [7] and look-up-tables (LUTs) [8]. This good performance is mainly generated by considering the memory effect of PA. Beyond its performance, the well-defined physical meaning of GMP is also a significant advantage.

The formulation of the GMP model is provided below:

$$\begin{aligned} y_{\text{GMP}}(n) = &\sum_{k=0}^{K_a-1}\sum_{l=0}^{L_a-1} a_{kl}x(n-l)\,|x(n-l)|^k \\ &+\sum_{k=1}^{K_b}\sum_{l=0}^{L_b-1}\sum_{m=1}^{M_b} b_{klm}x(n-l)\,|x(n-l-m)|^k \\ &+\sum_{k=1}^{K_c}\sum_{l=0}^{L_c-1}\sum_{m=1}^{M_c} c_{klm}x(n-l)\,|x(n-l+m)|^k\,. \end{aligned} \tag{2.2}$$

Here, K is the highest envelope power that is alias-free. L is the memory length. M is the inserted delayed memory length. l stands for the tapped delay, and m is the number of inserted delay samples. a_{kl},b_{kl}, and c_{kl} are coefficients, respectively, corresponding to the aligned signal and envelope, the signal and lagging envelope, and the signal and leading envelope. In practical application, GMP often keeps the odd order due to the characteristic of RF PA operating signals and the number of samples:

$$
\begin{aligned}
y_{\text{GMP}}(n) = & \sum_{\substack{k=0 \\ k \text{ odd}}}^{K_a-1} \sum_{l=0}^{L_a-1} a_{kl} x(n-l) \left|x(n-l)\right|^k \\
& + \sum_{\substack{k=1 \\ k \text{ odd}}}^{K_b} \sum_{l=0}^{L_b-1} \sum_{m=1}^{M_b} b_{klm} x(n-l) \left|x(n-l-m)\right|^k \\
& + \sum_{\substack{k=1 \\ k \text{ odd}}}^{K_c} \sum_{l=0}^{L_c-1} \sum_{m=1}^{M_c} c_{klm} x(n-l) \left|x(n-l+m)\right|^k .
\end{aligned} \tag{2.3}
$$

When we consider the input of I and Q separately, the number of parameters p_{GMP} of the GMP model referred to 2.2 is given as:

$$
p_{\text{GMP}} = 2K_aL_a + 2K_bL_bM_b + 2K_cL_cM_c \tag{2.4}
$$

K, L and M have the same definition as in 2.2.

2.4. Neural Network Architectures

This section introduces various NNs architectures applied to RF PA DPD, following the order presented in table 2.1. Neural networks based on Multilayer Perception (MLP) model are shown in subsection 2.4.1. Moving on to subsection 2.4.2, Deep Neural Networks (DNNs) with time-delay technique are introduced. Subsection 2.4.3 shows architectures based on basic recurrent neural networks (RNNs) and based on gated technique. Finally, subsection 2.4.4 contains the architectures based on Convolutional Neural Networks (CNNs).

Sec. 2.4.1:	Basic Multilayer Perception structure	
	Modified	Radial-Basis Function NN
Multilayer Perception	Multilayer Perception	Residual NN
Sec. 2.4.2:	Real-Valued Time-Delay NN	
	Augmented Real-Valued Time-Delay NN	
Time-Delay	Vector decomposition time-delay NN	
Neural Networks	Augmented Vector Decomposition Time-Delay NN	
Sec. 2.4.3:	Basic RNNs	
	Long-Short Term Memory	
Recurrent	Gated Recurrent Unit	
Neural Networks	Customized Cell	
Sec. 2.4.4: Convolutional Neural Networks		

Table 2.1: The structure of NN literature review Section 2.4.

2.4.1. Multilayer Perception: Feedforward Artificial Neural Networks

From the foundation of complex neural networks, MLP NN architecture is firstly widely applied for DPD. MLP is an artificial neural network structure having an input layer, one or more hidden layers, and one following output layer. It uses non-linearity activation to connect layers and uses the backpropagation technique for training. Figure 2.3 shows the structure of MLP.

MLP architecture is regarded as a basic NN architecture because it utilizes fully-connected feedforward Artificial Neural Networks (ANNs) structure. Moreover, MLP shows NN's ability to model non-linearity according to the universal approximation theorem [9].

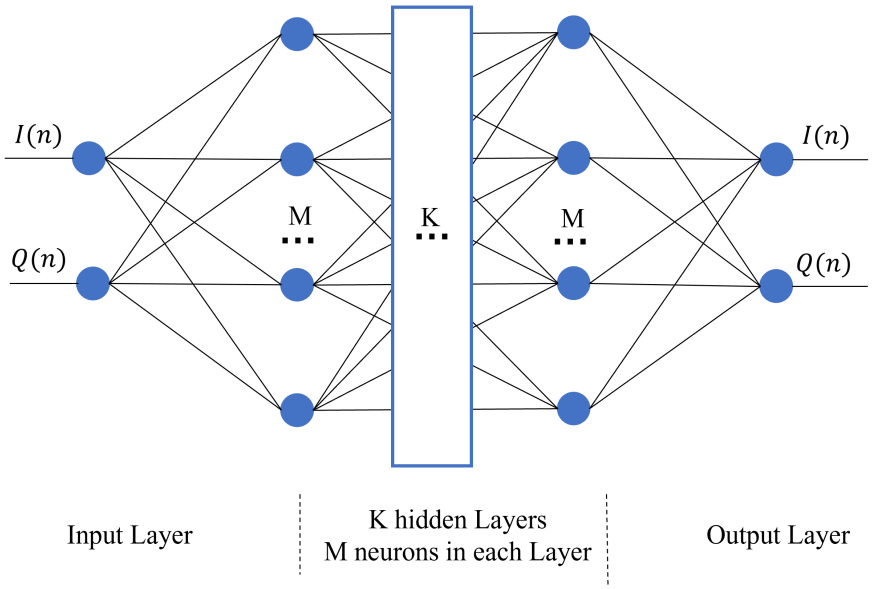

Figure 2.3: The general structure of MLP [10].

Researchers have experimented with various modifications on the MLP structures from the simplest model to achieve better performance. Two important techniques in DPD are introduced into MLP. The first one is to use different input layer structures. Figure 2.3 shows the most popular input choice in-phase and out-phase (I and Q) [11]. Amplitude and phase can be another input choice to consider AM/AM and AM/PM distortion rather than I and Q imbalance. The second technique is the shortcut [12], which connects the input layer and the output layer to make the hidden layers focus on non-linearity. The NN architecture built on the shortcut technique is named residual NN. Figure 2.4 shows the residual NN schematic.

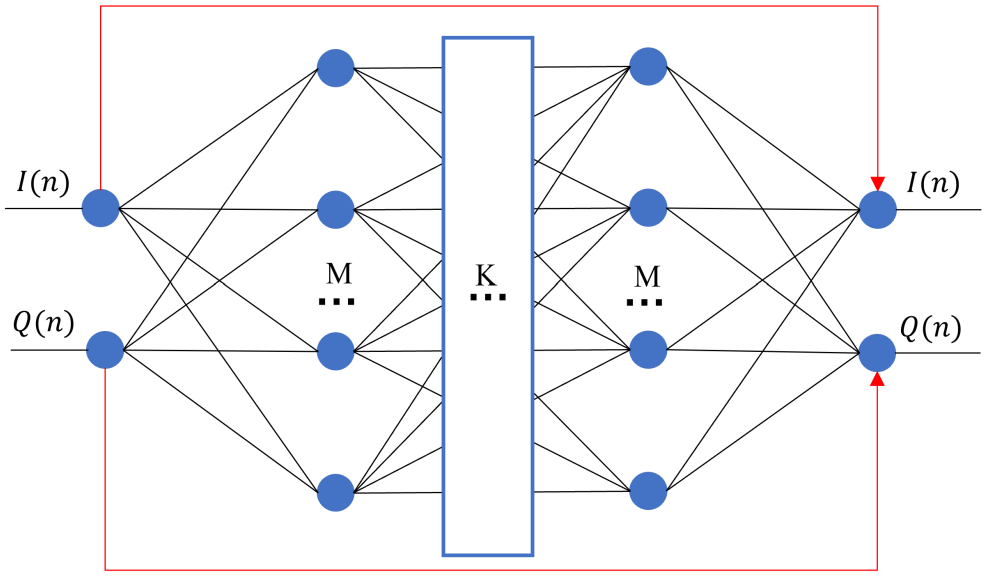

Figure 2.4: The general structure of residual MLP [13].

Other intuitive methods are also considered. For example, papers [10] and [14] utilized different sizes for input and output nodes. Paper [13] uses multivariate Gaussian function as transformation between the input layer and hidden layer rather than traditional activation function, such as sigmoid and tanh function.

In Figures 2.3 and 2.4, M is the number of neurons of each hidden layer. K is the number of hidden layers.

2.4.2. Time-delay Neural Networks

As for high-frequency and high-bandwidth operated signals in the 5G wireless system, the memory effect becomes more influential in DPD. Expanding the input signal of the MLP-based structure to a time-sequential signal is a valuable and direct way to consider the memory effect. This section shows five time-delay neural network (TDNN) structures: RVTDNN, augmented RVTDNN,residual real-valued time-delay neural network (R2TDNN),VDTDNN and augmented VDTDNN.

Paper [15] adds tapped delay lines in its I and Q inputs. Adding time-delay inputs is one of the ways to consider the memory effect in NNs. As shown in Figure 2.5, this structure also expands the number of hidden layers to two and considers the nonlinearity imbalance I and Q based on MLP. All these methods help to fit PA's nonlinearity more accurately.

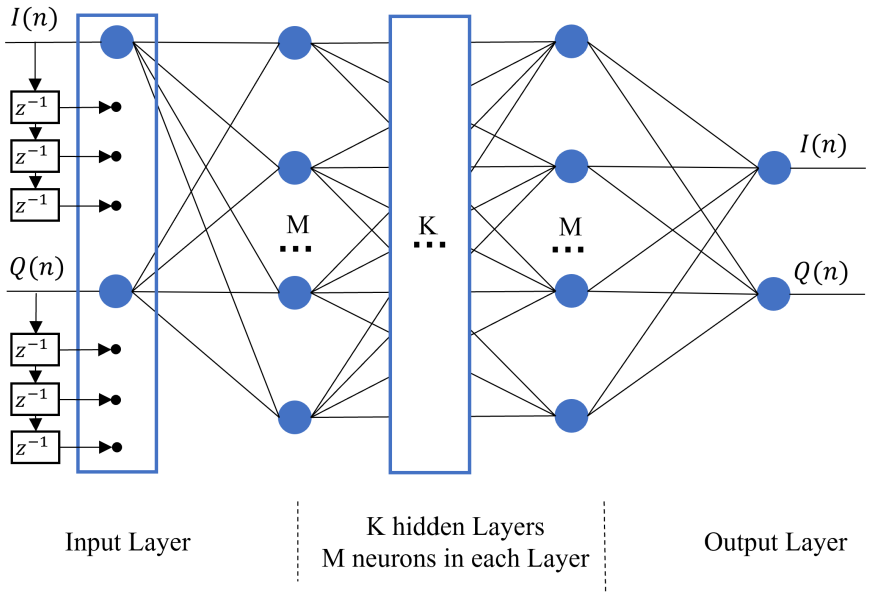

Figure 2.5: The block diagram of RVTDNN [15].

Based on the RVTDNN, the ARVTDNN [16] uses not only the time-delayed I and Q inputs but also time-delayed 1∼3th power order amplitude inputs. The architecture of ARVTDNN is shown in Figure 2.6. The R2TDNN [17] expands the number of hidden layers further, as well as adding the shortcut method is mentioned in residual NN in the section 2.4.1.

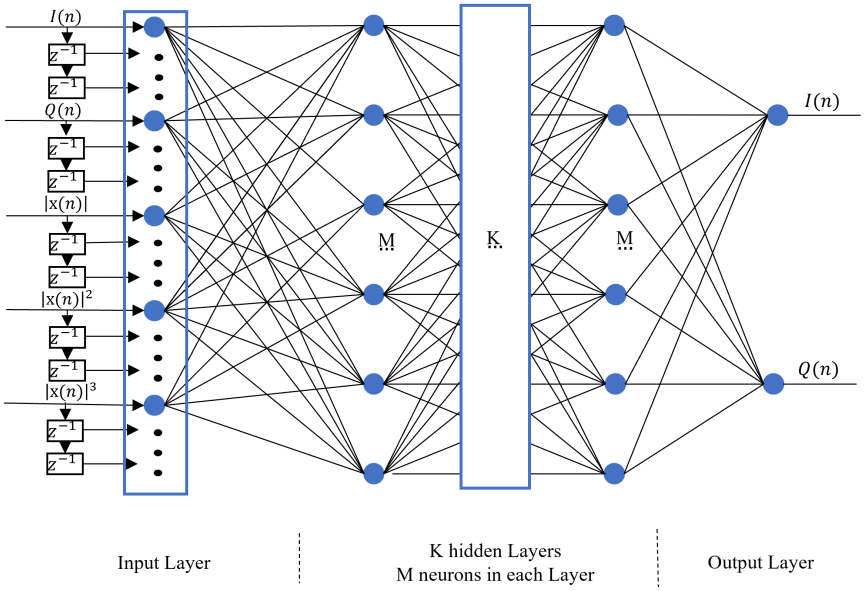

Figure 2.6: The block diagram of ARVTDNN [15].

On the other hand, paper [18] proposed the VDTDNN structure to use time-delay amplitude signals and then use a phase recovery layer to recover the phase information. The block diagram is shown in Figure 2.7.

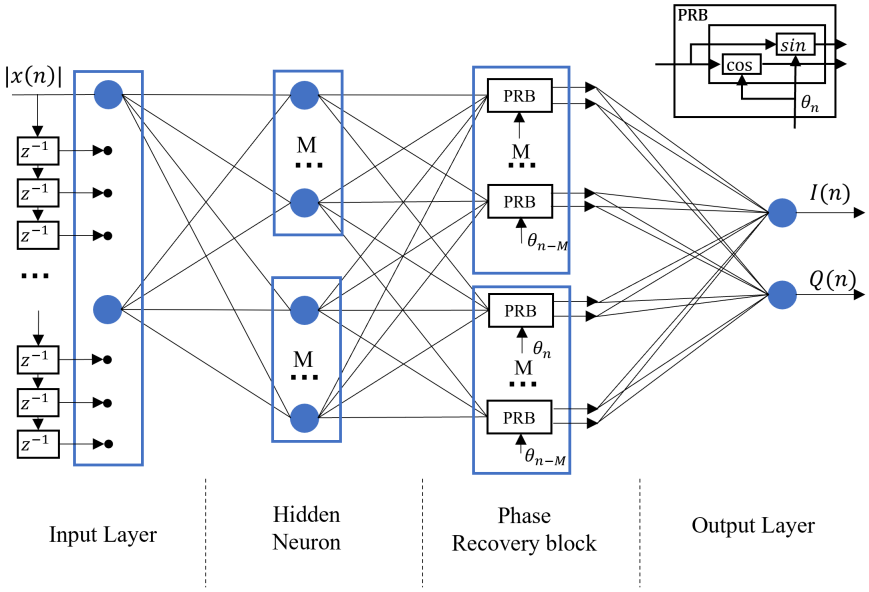

Figure 2.7: The block diagram of VDTDNN [18].

The VDTDNN has an augmented edition that utilizes higher power order time-delay amplitude inputs, named AVDTDNN. The phase recovery block is also modified by splitting the coefficients of the $cos(\theta)$ and $sin(\theta)$ parts. The combination of AVDTDNN and modified phase recovery block is shown in Figure 2.8.

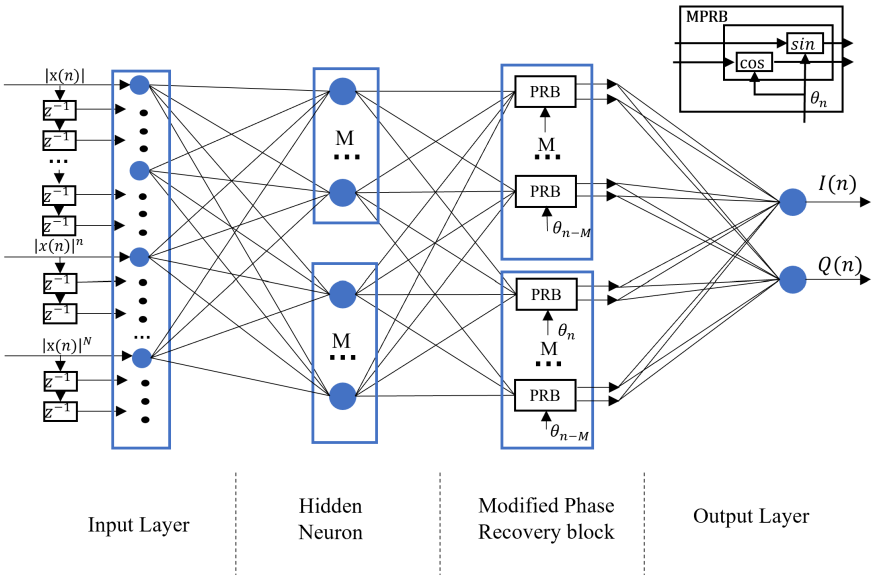

Figure 2.8: The block diagram of AVDTDNN [18].

2.4.3. Recurrent Neural Networks

As shown in Section 2.4.2, introducing techniques that consider the long-term memory effect from I/Q and amplitude aspects is one of the most important goals of TDNN. However, increasing the memory length in TDNN means expanding the number of neurons of the input layer, which can cause the number of coefficients to increase rapidly. This is non-ideal for both of the NNs complexity and hardware cost. To address this condition, RNNs are applied for RF PA DPD. RNNs can take infinite memory samples into account, which makes itself an efficient structure to model the nonlinearity of PA.

Besides, when we try to improve the performance by increasing the number of layers, deep layers in feedforward DNNs face vanishing gradient problems resulting from limited sensitivity and saturation of nonlinear activation. Gating techniques in RNNs are proposed to solve vanishing gradient problems and are now efficiently applied for RF PA DPD.

This section firstly introduces basic RNN applied to DPD. Secondly, two critical cells using gate techniques to control information flow through RNNs, LSTM, and gated recurrent unit (GRU) are introduced. Then four different architectures generated from these two cells and two architectures with customized cells are shown.

Basic RNN

RNNs add feedback connection on feedforward NNs. By taking the sequence-to-sequence regression mode, RNNs can adapt to different lengths of input time sequences using internal states while not affecting the number of parameters. The details of sequence-to-sequence regression mode are shown in sub-section 2.4.3. The paper [19] firstly implemented the Full recurrent neural network (FRNN) structure in RF PA DPD. The paper [20] adds IQ imbalance and tapped-delay line to the FRNN model to build a real value full recurrent neural network (RVFRNN). The block diagram of RVFRNN is shown in Figure 2.9. However, the experiment results of paper [20] observed that the recurrent neural network didn't perform better than the feedforward one. This can result from the direct connection of the feedback loop. Since feedback information without filtering can even hurt the performance, gate techniques gain the second reason to be applied for DPD.

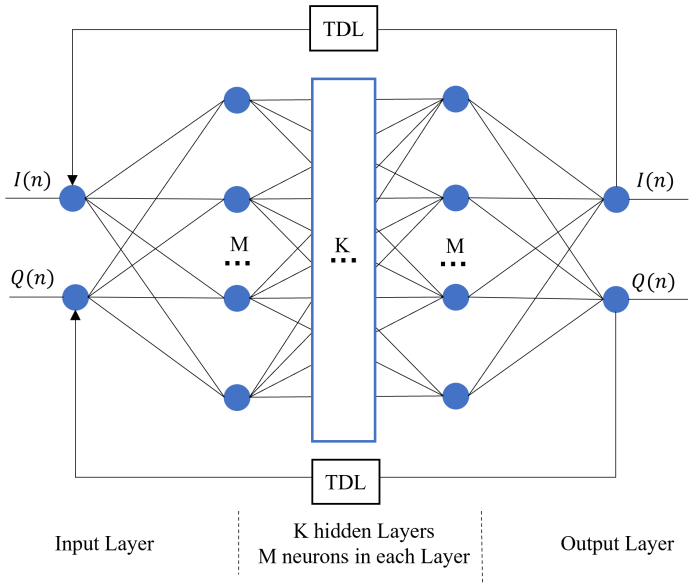

Figure 2.9: The block diagram of RVFRNN and RVFTDNN [20].

RNN with gating technique

The popular schematic for RNN with gating technique is shown in Figure 2.10. The input can be different types of input signals at present, such as $I(n)$ and $Q(n)$, or $amp(n)$, $cos(n)$, and $sin(n)$.

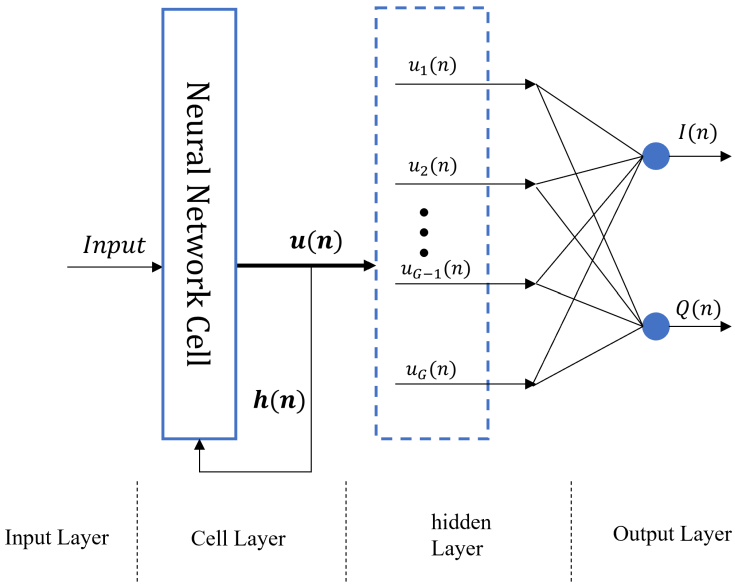

Figure 2.10: The common schematic of RNN with gating technique.

Two regression training modes are always used in RNN training. One is the sequence-to-one training mode. The other is the sequence-to-sequence training mode. During sequence-to-one training mode, the cell layer only generates one output vector $u(n)$ after all input time steps from $Input(n-T)$ to $Input(n)$. Then the output vector passes the fully connected to generate output. The progress of the sequence-to-one regression mode is shown in Figure 2.12. T stands for the length of every training sequence.

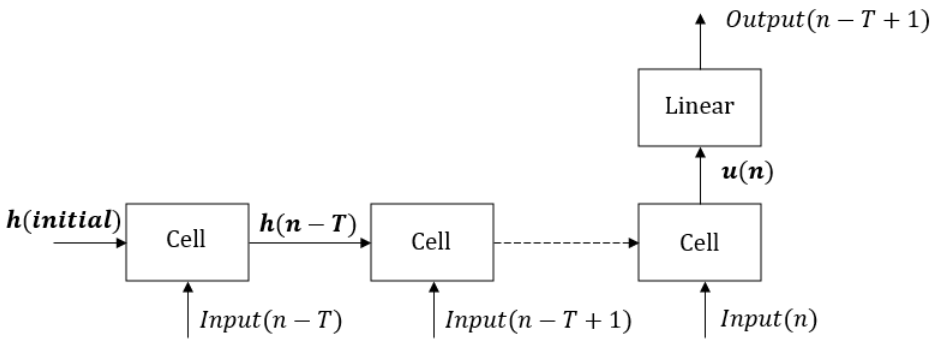

Figure 2.11: The progress of sequence-to-sequence regression mode.

During sequence-to-sequence regression training mode, every time the input passes through the cell layer, the cell layer generates an output vector $u(n-T)$ for this time point and a hidden activation $h(n-T)$ for the next time point. Every output vector $u(n)$ is fully connected to the output layer to generate the final output at this time point. The hidden activation is fed back to help the next time point to collect information from this time point. After all input signals during the sequence pass through the cell layer, an out layer with the sequence length is built. Finally, We minimize the mean square error (MSE) between output and target to optimize the parameters in NN. The progress of the sequence-to-sequence regression mode is shown in Figure 2.12. T still represents the length of every training sequence.

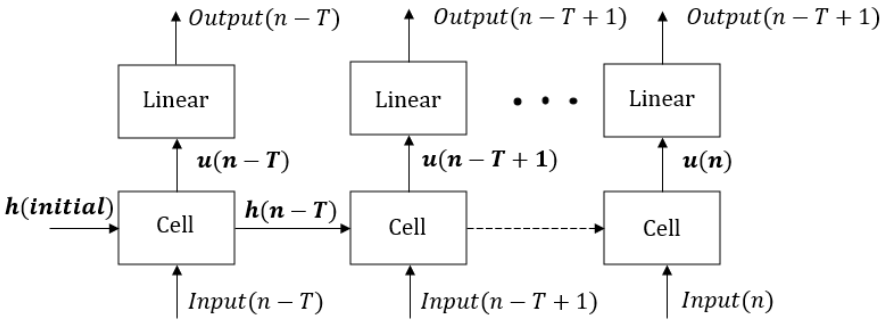

Figure 2.12: The progress of sequence-to-sequence regression mode.

The cell layer is the core layer in gated RNNs, which helps to capture the long-term memory effect of PA. Being different from direct feedback on all information, gated input in the cells determines how the input information is forgotten, preserved, and updated to output information. Therefore, the details of the cells should be clarified. LSTM and GRU are two main kinds of RNN cell layer. The LSTM cell schematic is shown in Figure 2.13 and the GRU cell schematic is shown in Figure 2.14.

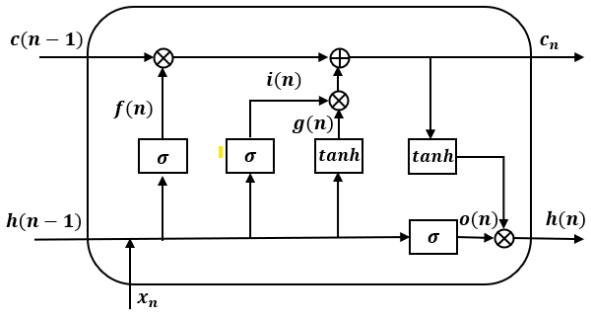

Figure 2.13: The schematic of LSTM cell.

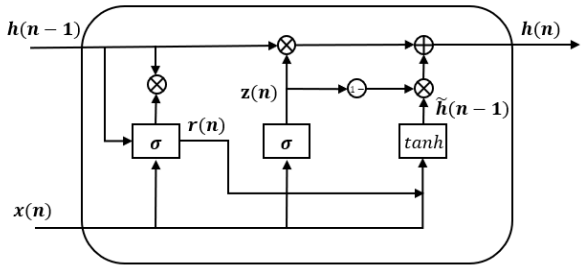

Figure 2.14: The schematic of GRU cell.

As shown in Figure 2.13 and 2.14, both LSTM and GRU cells contain a ”forget gate layer” to determine forgetting part and preserving part of past information, a ”reset gate layer” to update new information, and an ”output layer” to decide how to output information. Corresponding to the symbol in two Figures, the formulations of LSTM cell are given as:

$$\mathbf{f}(\mathbf{n}) = \sigma(\mathbf{W}_f\mathbf{x}(\mathbf{n}) + \mathbf{R}_f\mathbf{h}(\mathbf{n}-\mathbf{1}) + \mathbf{b}_f) \tag{2.5}$$
$$\mathbf{g}(\mathbf{n}) = \tanh(\mathbf{W}_g\mathbf{x}(\mathbf{n}) + \mathbf{R}_g\mathbf{h}(\mathbf{n}-\mathbf{1}) + \mathbf{b}_g) \tag{2.6}$$
$$\mathbf{i}(\mathbf{n}) = \sigma(\mathbf{W}_i\mathbf{x}(\mathbf{n}) + \mathbf{R}_i\mathbf{h}(\mathbf{n}-\mathbf{1}) + \mathbf{b}_i) \tag{2.7}$$
$$\mathbf{o}(\mathbf{n}) = \sigma(\mathbf{W}_o\mathbf{x}(\mathbf{n}) + \mathbf{R}_o\mathbf{h}(\mathbf{n}-\mathbf{1}) + \mathbf{b}_o) \tag{2.8}$$
$$\mathbf{c}(\mathbf{n}) = \mathbf{f}(\mathbf{n}) \otimes \mathbf{c}(\mathbf{n}-\mathbf{1}) + \mathbf{i}(\mathbf{n}) \otimes \mathbf{g}(\mathbf{n}) \tag{2.9}$$
$$\mathbf{h}(\mathbf{n}) = \mathbf{o}(\mathbf{n}) \otimes \tanh(\mathbf{c}(\mathbf{n})) \tag{2.10}$$

The formulations of GRU are given as:

$$\mathbf{z}(\mathbf{n}) = \sigma(\mathbf{W}_z\mathbf{x}(\mathbf{n}) + \mathbf{b}_z) \tag{2.11}$$
$$\mathbf{r}(\mathbf{n}) = \sigma(\mathbf{W}_r\mathbf{x}(\mathbf{n}) + \mathbf{b}_r) \tag{2.12}$$
$$\tilde{\mathbf{h}}(\mathbf{n}-\mathbf{1}) = \tanh(\mathbf{W}_h\mathbf{x}(\mathbf{n}) + \mathbf{U}_h(\mathbf{r}(\mathbf{n}) \otimes \tilde{\mathbf{h}}(\mathbf{n}-\mathbf{1})) + \mathbf{b}_h) \tag{2.13}$$
$$\mathbf{h}(\mathbf{n}) = (1 - \mathbf{z}(\mathbf{n})) \otimes \mathbf{h}(\mathbf{n}-\mathbf{1}) + \mathbf{z}(\mathbf{n}) \otimes \mathbf{h}(\mathbf{n}) \tag{2.14}$$

The first difference between LSTM and GRU cells is that candidate activation $h(n)$ affects the final memory maintained in LSTM cell. On the contrary, the previous activation $h(n-1)$ is independent of the candidate activation $h(n)$ in GRU. The second one is that the previous activation is directly introduced into the memory cell in the LSTM cell, while the GRU cell controls the amount of information flowing from the previous time step by the reset gate r. The last is:

LSTM has an independent forget gate and input gate, while the forget gate is one minus the input gate in GRU Model [21].

According to the special function of the LSTM cell shown in Figure 2.13, the paper [22] uses LSTM cells as a core layer of NN with a tap-delayed I and Q input layer, a batch normalization layer, an attention layer, and a full-connected output layer. Paper [23] and paper [3] also utilize LSTM cells. The special variation in paper [23] is trying the bidirectional LSTM cell to consider the memory effect from two directions. The structure in paper [3] changes the fully connected layers between the input and phase recovery in VDTDNN to a recurrent LSTM cell to fit the vector decomposition input into the LSTM architecture.

For GRU cell, Paper [24] uses modified GRU cells as core layers to build an RNN as shown in Figure 2.15.

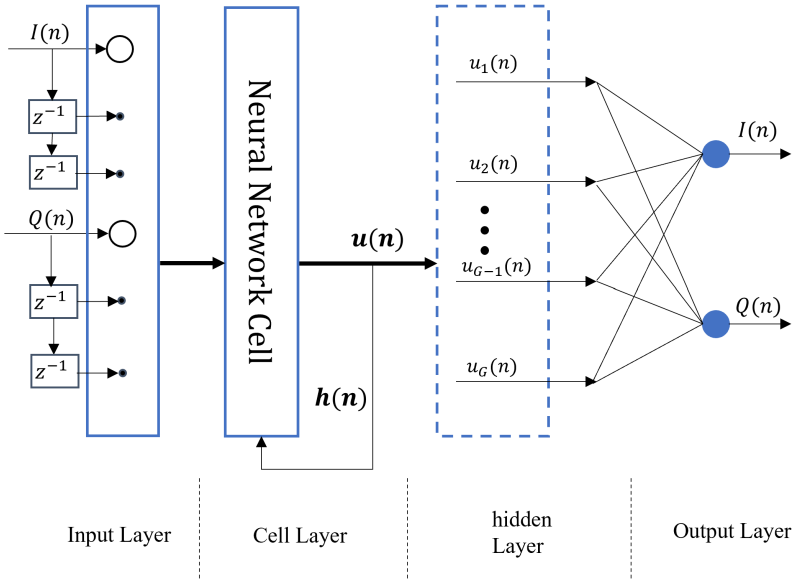

Figure 2.15: The structure of GRU layer [24].

To save energy for DPD, the GRU cell in paper [24] is modified and simplified to IGIRNN cell, which means the candidate activation $h(n)$ does not depend directly on input but utilizes the input information from the previous activation $h(n-1)$ indirectly. However, IGIRNN uses tapped delay line input, which dramatically increases the number of neurons in the input layer. It's not an ideal choice because the function of the tapped delay line overlaps the function of RNN.

When implementing RNN in DPD, some architectures also try to solve the problem from the AM/AM and AM/PM perspectives. Paper [1] tried another way to deal with the imbalance between amplitude and phase. It decomposes the input into the amplitude part and phase part and then lets them pass through the "update gate," respectively. The customized cell named just-another-network (JANET) [25] simplifies the GRU cell by keeping the "update gate layer" and "output gate layer" only.

All architectures mentioned use a relatively traditional way to deal with the nonlinearity of signal. The non-linearity learning capability mainly depends on the number of layers, the activation function, and the recurrent gate. To improve the non-linearity learning capability without increasing the number of parameters, paper [2] introduces a powerful technique named decomposed vector rotation (DVR) to the input of JANET architecture. DVR method has two main differences from conventional methods. The first is it introduces three thresholds for linear weighted amplitude. This makes sense for wireless systems where the non-linearity varies for different amplitude intervals. The second difference is that it considers different kinds of

amplitude and phased memory effects and their influence on each other.

For the complexity of DPD models, RNN is not the ideal choice to decrease the number of coefficients, especially when the architecture uses time-delay input like IGIRNN. However, both IGIRNN and PG-JANET show that finding other ways to extract input features helps to achieve better performance. This upper bound of the nonlinearity modeling capability is much higher for RNNs compared with GMP. On the other hand, DVR-JANET remarkably decreases the number of coefficients in the cost of processing complexity.

2.4.4. Convolution Neural Networks

As another major branch of neural networks, convolution neural networks have also been considered since the running speed of DPD and the area has become increasingly important. Paper [26] proposed a two-dimensional real-value time-delay convolution neural network (RVTDCNN) structure, whose architecture is shown in Figure 2.16.

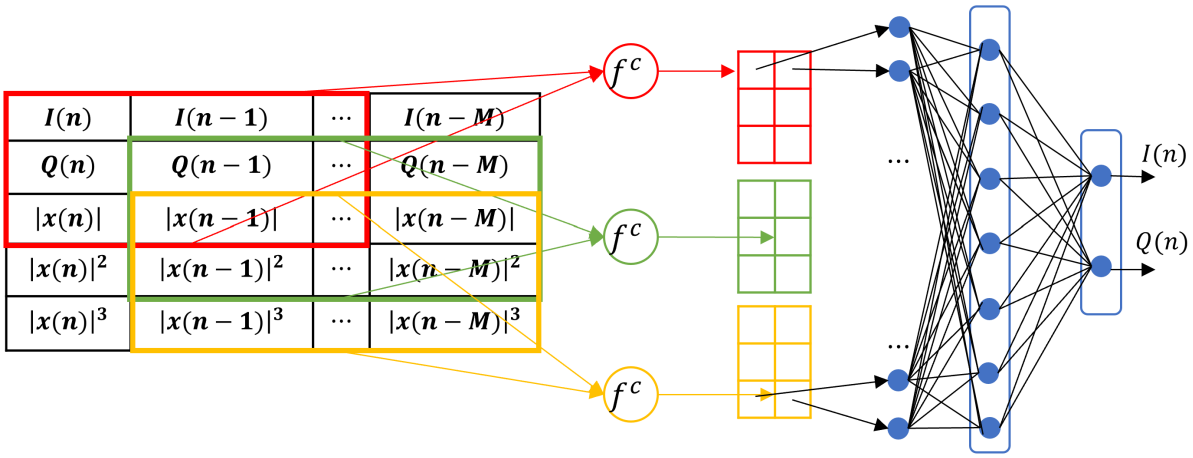

Figure 2.16: The architecture of RVTDCNN [26].

The RVTDCNN makes features and tap-delay points two-dimension matrix so that the Convolutional Neural Network (CNN) can capture the relationship between features and short-term memory as a local characteristic. When PA has a short memory effect, the RVTDCNN can significantly decrease the number of parameters.

2.5. Learning Architectures

Learning architecture is the method that determines how to extract DPD parameters. The target of all different learning architectures is to make the output of DPD get close to the ”real” ideal input of PA. This ideal input of PA compensates as much as PA nonlinearity. Therefore, the different learning architectures used to extract parameters of DPD have an impact on the NMSE and ACPR performance and the consistency between NMSE and ACPR. It should be determined carefully when training NN based DPD model. This section gives an introduction to popular learning architecture, ILA, DLA, and ILC.

2.5.1. Indirect Learning Architecture

ILA tries to model the inverse function of PA. During training, it uses the down-converted output $\frac{y(n)}{G}$ of PA as the DPD input and uses the PA input $u(n)$ as DPD output. The scheme of ILA is shown in Figure 2.17. ILA is a simple method compared to the DLA and ILC. However, we assumed that the PA model has a valid commutation under this condition. This assumption does

not hold in practice. On the other hand, measurement noise and limited feedback bandwidth affect the accuracy of the predistorter.

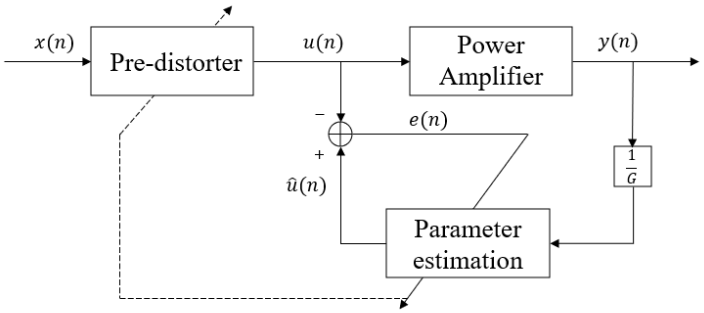

Figure 2.17: Scheme of ILA [27].

2.5.2. Direct Learning Architecture

DLA firstly have a close model of the PA itself based on the collection of the PA characteristic information. By combining this PA model with the NN-based DPD model, the system pushes its output signal to the linear amplified input signal. When the training system has a relatively accurate PA model, and the error is small enough. The output of the DPD is the ideal input of the PA. The DLA scheme is shown in Figure 2.18. Under this condition, we need more information about PA itself [28].

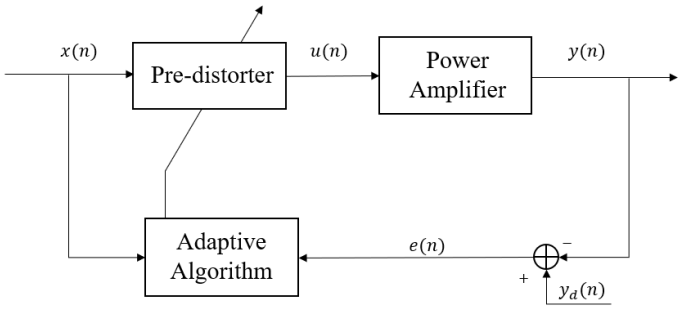

Figure 2.18: Scheme of DLA [27].

2.5.3. Iterative Learning Control

The key idea of ILC-based DPD is to evaluate an optimal PA input that can generate the ideal PA output. After selecting the ideal output signal of PA, the ILC learning algorithm guarantees that the newly calculated input generates a smaller error between the output and the ideal output. ILC-based learning architecture can be used to directly get the ideal input or be a step before DLA as shown in Figure 2.19.

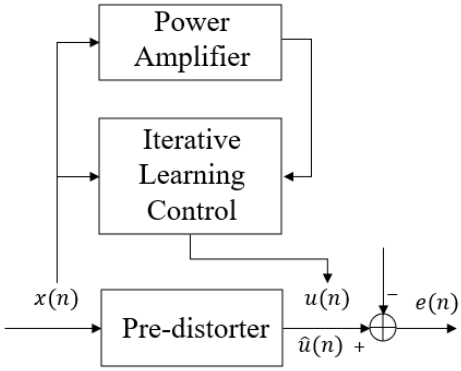

Figure 2.19: Scheme of ILC [29].

For basic ILA and DLA, papers [27] and [29] showed that DLA works best, then ILC, then ILA based on Memory polynomial (MP) or GMP model. DLA has the best performance by increasing the complexity of the identification process.

2.6. Validation Experiment Platforms

No matter what learning architecture is used, the data pair used for the training DPD model can not exhaust all input and output situations of a real PA. Moreover, under DLA and two-step learning architecture, calculating ideal inputs will also introduce errors. These reasons cause that NMSE performance can't stand for ACPR performance. A validation platform is used to verify this consistency between model convergence performance and adjacent channel power suppression performance. The validation platform has main components shown in Figure 2.20: DPD, DPD parameter extraction, signal generator, Digital-to-Analog converter (DAC), up-conversion, PA, Analog-to-Digital converter (ADC), down-conversion, spectrum analyzer, and attenuator. Taking into account how these components are implemented, DPD verification platforms are divided into three types.

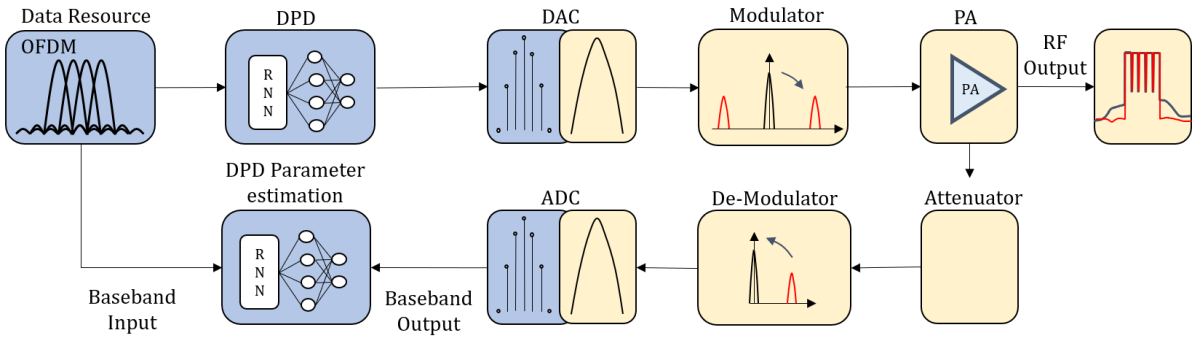

Figure 2.20: A schematic diagram of a validation platform.

The first one is simulation software based DPD. This type of DPD relies on the computational ability of MATLAB/PyTorch. A corresponding mathematical model implements all the steps of validation. PA is a coefficients matrix simplified from a real PA in this validation type. Based on PA characteristic simplification, proposed DPD NN architecture working well on the simulation platform is the foundation of validation on real PA.

The second is commercial measurement and instruments based on DPD. This type utilizes a commercial signal generator and a spectrum analyzer with digitizing capability. The data pairs also come from commercial PA while DPD parameter extraction and DPD are still finished

on a personal computer.

The final type is the digital and analog hardware evaluation board-based DPD platform. For example, FPGA is popular for achieving board-based DPD. The second and third validation platform types are more popular for the NNs based DPD.

2.7. Comparison and Argumentation

This section first compares the NNs architectures from operating signal bandwidth, NMSE, ACPR, and theoretical computation complexity. Second, we show the comparison difficulties caused by learning architecture and validation platforms. Third, we analyze the reason for performance differences to emphasize important factors in the NN DPD structures design and validation. Finally, we list some existing questions and look forward to possible future developments.

2.7.1. Performance Comparison

To control the variables and avoid potential influence, the architectures, and experiment results are chosen to show in Table 2.2 following these four rules:

1. All come from the 100 MHz test signal. The 100 MHz test signal is a fair wide-band signal suitable for the 5G wireless system application. Furthermore, the test signal bandwidth has an obvious impact on both NMSE and ACPR performance according to work [1] and [2].

2. They are tested on four specific experiment platforms. These results are obtained from the papers [1] [2] [24] [26] instead of the original paper that proposed the corresponding architecture. Moreover, PG-JANET and DVR-JANET should have very similar experiment environments so that at least two groups can be compared relatively accurately.

3. We show improved ACPR and relative coefficients of different NN architectures compared to the GMP model given in their corresponding articles. These two metrics are shown to try to decrease the influence of different PAs, RF, and sampling rates.

4. The architecture should have special techniques to deal with PA non-linearity.

Type			Model	NMSE (dB)	Relative ACPR(%)	#Coef.	Relative Coef.
MLP			DNN [30]	-36.42	-17.67	801	0.7
	Tapped -Delay	Real -Value	RVTDNN [15]	-35.09	-14.8	387	1.8
			ARVTDNN [16]	-36.47	-18.52	393	1.8
		Vector -Decomposed	VDTDNN [18]	-37.59	19.71	12202	85.9
			AVDTDNN [18]	-39.59	53.15	1506	0.9
RNN			RNN [24]	-37.21	17.92	13600	63.6
	Gated RNN		LSTM [31]	-36.27	-17.23	467	2.2
	Online Feature Extraction		VDLSTM [3]	-41.88	-3.44	1532	0.9
			IGIRNN [24]	-41.09	-23.88	14100	99.3
			PG-JANET [1]	-43.42	-7.69	1514	0.9
			DVR-JANET [2]	-40.27	-30.68	509	1.5
CNN			RVTDCNN [26]	-36.44	-21.6	801	0.7

Table 2.2: Comparison of results when the test signal is 100 MHz OFDM signal. Relative ACPR equals $\frac{Model-GMP}{GMP}$.Relative coefficient equals $\frac{Model}{GMP}$ The improved ACPR is compared to the GMP model in the following referred paper. Data of VDTDNN,RNN and IGIRNN are referred to paper [24]. Data from AVDTDNN,VDLSTM and PG-JANET are referred to paper [1]. Data for DNN, RVTDNN, ARVTDNN, LSTM, RVTDCNN are referred to paper [26]. Data of DVR-JANET is referred to paper [2].

Firstly, we directly compare the value shown in Table 2.2. Here, VDTDNN, RNN, and IGIRNN shown should be considered weaker because their number of coefficients is too large than ground GMP while only IGIRNN generates better ACPR results. The model PG-JANET shows the best NMSE results and also shows the highest efficiency to improve NMSE results by adding coefficients. Model DVR-JANET shows the best relative ACPR compared to the baseline model. RVTDCNN shows the best efficiency in improving ACPR by adding coefficients. At the same time, what should be mentioned is that the paper [26] uses +/- 20 MHz as adjacent channels. This calculation can affect ACPR results. Even if it cannot be determined whether this improved ACPR is a valid metric or not, these data still reflect the improvement in the performance of the NN structure compared to the traditional structure in a sense.

Secondly, the techniques of different models are analyzed on the basis of performance.

- Real-Valued Time-Delay input: The biggest advantage of real-valued TDNN is their low complexity. This advantage can be further enhanced by combining with CNN.
- Vector decomposition: The performance difference between real-valued TDNN and vector-decomposed TDNN shows that vector decomposition is not efficient in feedforward models. With a larger number of coefficients, vector-decomposed models generate worse ACPR.
- Gated RNNs: Gated RNNs with input feature extraction layer show the best NMSE and ACPR improvement performance. They also control the number of coefficients efficiently. However, the complicated processing can be problematic when applied to hardware.

Some prior work mentioned training time as one of the metrics. We didn't consider it a major metric because it is assumed that the digital pre-distorter only needs a few times training processes during its lifetime. Finally, even if CNN performed well from the number of coefficients with good ACPR performance, this statement can be overturned if we want to pursue a higher NMSE and use an input layer with higher memory depth. The paper [26] only considered the memory depth of 2 to 5. The number of coefficients can not stay competitive when the memory depth increases. The assumption that increasing memory depth can help increase NMSE is based on the result of the paper [24]. Under the same definition of memory depth, IGIRNN gave much better NMSE with 15 memory depth and a simple input I/Q.

2.7.2. Key Factors in NNs Architecture

This subsection will analyze the critical points in NNs models and the training process that affect DPD performance. These factors should be carefully determined in future work.

- Feature selection: The RF PA model contains both IQ and amplitude/phase imbalance. Some models put their focus on IQ imbalance, which takes two advantages. First, the I and Q data are easier to collect in practice. Second, using I and Q as input features lets models waive complex coefficients. Amplitude and phase also have the real-valued coefficient advantage but are weak in preprocessing. They need to calculate more resources in the hardware design. As for performance, the amplitude and phase feature method "vector decomposition" shows better results when they are applied to RNNs, such as VDLSTM and PG-JANET, than MLP-based NNs, such as VDTDNN and AVDTDNN.
- Tapped-delay signal: Tapped-delay input signal and the tapped-delay feedback signal is a direct way to consider memory effect in MLP-based model. With a large memory length, the tapped delay method causes a long delay between input and output and rapidly increases the number of coefficients. In RNN, adding tapped delay isn't a good choice because of the above disadvantages and its function overlapping with the feedback loop.

- Augmented input: Whether to introduce the higher order magnitude and how to introduce the higher order magnitude should be determined for DPD. Models ARVTDNN, AVDTDNN, and RVTDCNN used augmented structures. It helps to learn the non-linearity of the model more accurately at the cost of the complexity of the model.
- Feature extraction: DVR-JANET and PG-JANET get their good results from more complicated feature preprocessing routes before the input features pass the RNN. Considering different ways to add other features and extract relevant features can be the key point of improving NN-based DPD performance. Moreover, two JANET based architectures are built by introducing the physical characteristic of PA into the input of RNNs, which can be one of the efficient ways to find the most suitable cell.
- Structure of a gated RNN cell: The difference in results between the LSTM-based model and the GRU-based model verified the way that forgetting and updating information affects DPD performance and complexity. Two GRU-based models showed that simplifying in cells can help reduce complexity without too much performance degradation. The competitive results of PG-JANET and DVR-JANET. On the one hand, show the validation of a simpler cell structure JANET.
- Skip-connection: Radial-Basis Function Neural Network (RBFNN) structure introduced a direct connection between the input and output layer. This method is also used in ARVTDNN, which helps the hidden layer to focus on non-linearity.
- Activation function: The choice of activation function in the feature extraction layer, the input layer, and the output layer can be one of the factors that affect performance. In VDTDNN model experiments, the activation function does not significantly affect the performance after adding linear terms. However, 1D-CNN in paper [32] prefers ReLU6 over the sigmoid function for CNN models. RVTDCNN in paper [26] prefers $Tanh$ activation function.
- Learning architecture: From the characteristics of different learning architecture, the main advantage of ILC is its simplicity. However, the experimental results show it was not competitive NMSE. Taking into account the performance metrics, first, the DLA may be preferred in future work.
- Validation details: Many technical details in the validation steps can influence the final performance. For example, OFDM modulation settings, sampling rate, basic linear PA performance, and radio frequency can all be the reasons for variances in performance results.

2.8. AI-based DPD Summary

To summarize, this section compared 15 different NNs models applied for the DPD of RF PAs. This comparison helps to find issues of previous work and future challenges. The first problem exposed in the comparison is that we don't have fixed experimental variables. Even if all the works show their NMSE and ACPR results, it is hard to determine that the better results are generated by the better NN architecture. Too many variables can affect the DPD results: learning architecture, tested PA, signal generating method, and training process. The absolute value of NMSE and ACPR can show conflict when the training process is not 100% clarified, especially for RNN. Moreover, the number of coefficients and the complexity of the calculation should be one of the most important metrics when DPD is implemented on the hardware. A new standard should also be considered to ensure that increasing the number of coefficients is worth increasing performance or that decreasing the number of coefficients has a better influence on hardware.

3 Methods

This chapter explains the methods of the proposed DPD learning framework. Firstly, Section 3.1 introduces E2E learning architecture. The learning architecture offers ideas to find unknown ideal input of PA and suitable parameters for DPD. Secondly, the motivation, the mathematical details, and the evaluation of the proposed SGRU architecture are shown in Section 3.2. Finally, we analyze the selected features in 3.3.

3.1. E2E Learning Architecture

Our project is the first to apply E2E learning architecture to RNN. Figure 3.1 shows that the E2E learning architecture has two steps. The first step is generating a baseband input signal and collecting output data from RF PA.

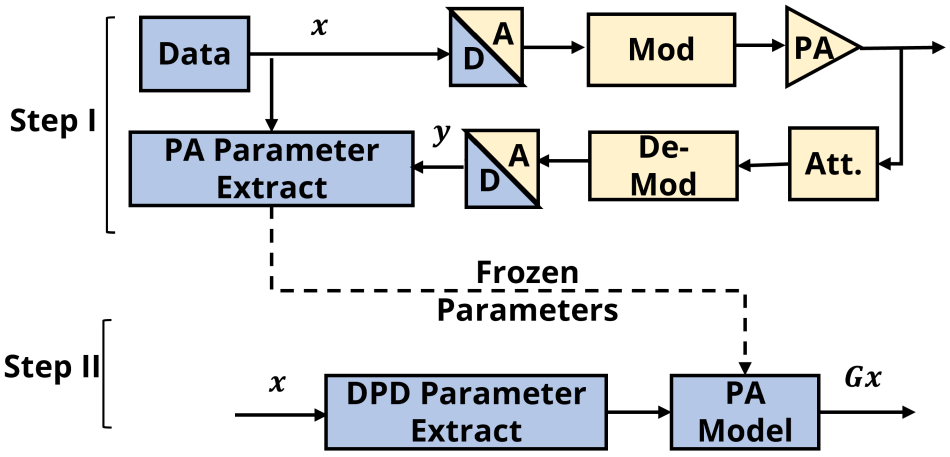

Figure 3.1: Stages of E2E learning architecture.

For the OFDM signal, the generating process is shown in Figure 3.2. We set the number of subcarriers in one channel, the FFT length as K, the guard band length as G, the number of pilot values as P, and the QAM type as M. While generating the multi-channel OFDM signal, we first generate a $K - 2 * G - 1 - P$ random integers in $[1,\ M]$ for each channel. According to the QAM constellation map, we find the corresponding complex value for each subcarrier and transfer it to the time domain by Inverse Fast Fourier Transform (IFFT).

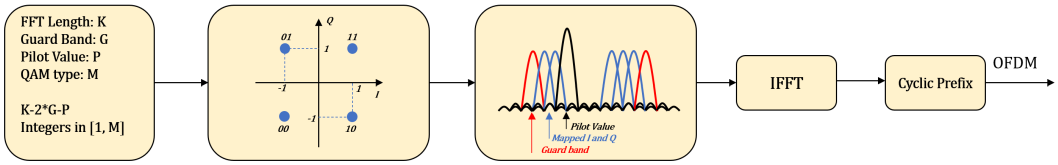

Figure 3.2: OFDM signal generation process.

Based on the one channel OFDM signal generation, We can get a multi-channel OFDM signal by adding signals of different channels together after up-converting to different radio frequencies.

After we get the training data set, we use it to build a PA transfer model using a NN. The input signal x and output target signals $\hat{y}$ are baseband input and output signals collected from the measurement instrument. With small simulated NMSE, a digital model with acceptable accuracy of the PA measurement system can be built. Then we froze the PA model parameters in the first step and connected the DPD training block to it. During the second step, the linear downconverted output signal $\frac{\hat{y}}{G}$ passes DPD and PA to try to generate the output signal $\hat{y}$. While the output of PA is converging to $\hat{y}$, the system is becoming more and more linear. The output of DPD finally converges to an ideal input of PA because the system is almost linear, and the digital PA model is very close to the real PA.

This learning architecture avoids ILA's assumption that the PA system is commuted. Moreover, compared to traditional DLA, the biggest advantage of this learning architecture is an easier way to find PA model. Finally, E2E learning architecture used an intuitive and simple logic to find the ideal input of PA, avoiding ILC and transferring signal multiple times between personal computer (PC) and the measurement instrument.

3.2. Proposed RNN Architecture

In this section, we first analyze the behavior of RF PA to emphasize the function of DPD unit. Secondly, We propose our RNN DPD architecture based on the requirements.

3.2.1. Analysis of RF Power Amplifier

The power transfer function of an RF PA can be visualized as Figure 3.3 a). Three components comprise the nonlinearity of an RF PA. The first is the memory effect, which brought the red dotted line various outputs in 3.3 a). The second is a non-linear trend before saturation, which multiple combinations may cause. The third is the gain clip after saturation. In most cases, the amount of gain compression that DPD can handle is limited, so we combine the first and second types. The combined non-linear trend is the blue curve in 3.3 a).

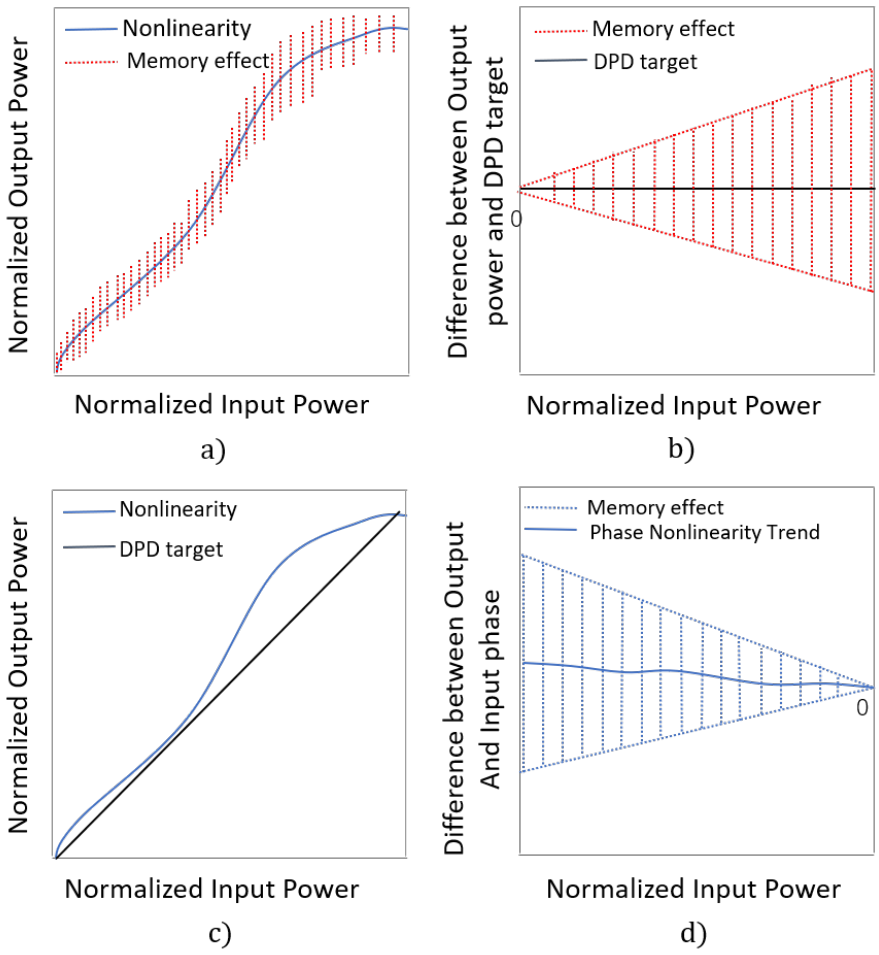

Figure 3.3: schematic diagram of RF PA nonlinearity: a) The power transfer function of an RF PA. b) Memory effect of an RF PA vs. Normalized Input power. c) Output Power vs. Normalized Input Power. d) Difference between Input and Output of PA vs. Normalized Input power.

Due to the memory effect, an RF PA will produce different outputs under the same input. Figure 3.3 b) shows the difference between the varying output and the ideal output as a function of the normalized input power. The nonlinear relationship between input and output power is expressed in Figure 3.2 c). With increasing PA input power, the gain of PA compresses and then saturates. Specifically, the nonlinear trend of an RF PAs means they have different gains with input power changing. By complementing nonlinear trends in Figure 3.2 a) and 3.2 b), the DPD unit can improve the ACPR performance of PA output signal.

However, the transferring signal is always complex, which means amplitude is affected by nonlinearity, and the phase between input and output signals also changes along the input power. To consider the phase nonlinearity shown in Figure 3.3 d), DPD helps to improve the system's EVM performance.

According to the characteristics of the transfer function of an RF PA, We proposed a RNN-based architecture have three functions: (1) The proposed architecture has a specific structure to concentrate on modeling the memory effect. (2) The proposed architecture can model the varying gain trend between output and input power. (3) The proposed architecture considers characteristic information, concluding amplitude, phase, and complex vector information.

3.2.2. Architecture of SGRU

The proposed SGRU model is shown in Figure 3.4.

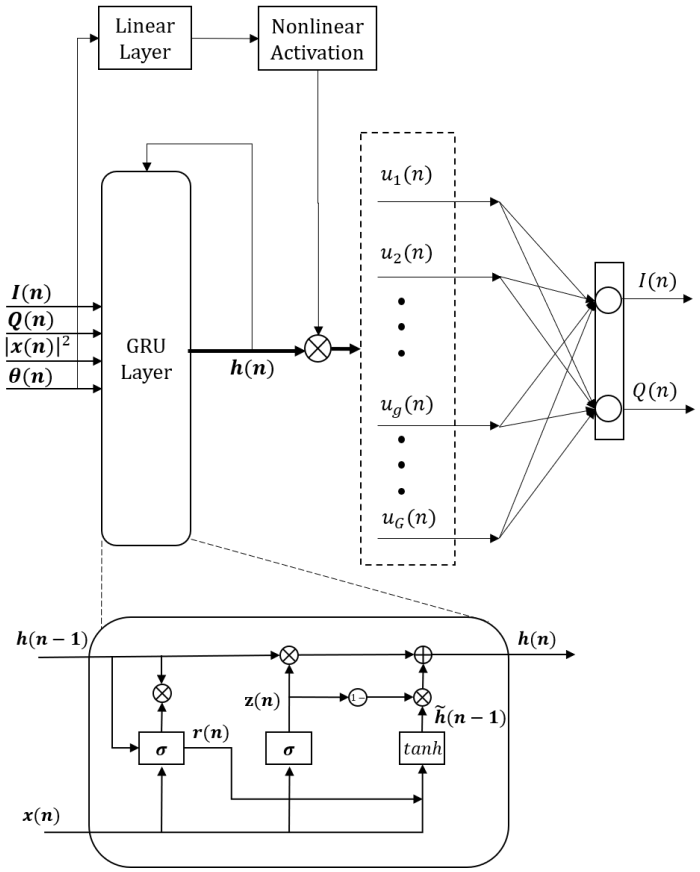

Figure 3.4: Schematic of SGRU model.

This model has three layers, one input layer, one GRU layer, and one fully connected output layer. The input layer has four parallel input features $I(n), Q(n), |x(n)|^2$, and $\theta(n)$. $I(n)$ and $Q(n)$ are used to offer information about modulation constellation so that the DPD unit can find corresponding output to improve EVM. $|x(n)|^2$ is the feature to offer amplitude information. $\theta(n)$ is the feature to offer phase information. During sequence-to-sequence training, the GRU layer saves all relevant information from previous time steps of input features and helps to find the relationship between output and input memory. The output layer combines the hidden states of each time step to generate I and Q output sequences linearly. To make the GRU cell concentrate on the complicated memory effect, a skip path is added to model the nonlinearity trend.

The proposed SGRU operation function is shown in 3.7.

Here $\mathbf{Feat(n)} = [\mathbf{I(n)}, \mathbf{Q(n)}, \mathbf{|x(n)|^2}, \theta(\mathbf{n})]$

$$\mathbf{z}(\mathbf{n}) = \sigma(\mathbf{W}_z\mathbf{Feat}(\mathbf{n}) + \mathbf{b}_z) \tag{3.1}$$
$$\mathbf{r}(\mathbf{n}) = \sigma(\mathbf{W}_r\mathbf{Feat}(\mathbf{n}) + \mathbf{b}_r) \tag{3.2}$$
$$\mathbf{h}(\mathbf{n}-\mathbf{1}) = \tanh(\mathbf{W}_h\mathbf{Feat}(\mathbf{n}) + \mathbf{U}_h(\mathbf{r}(\mathbf{n}) \otimes \mathbf{h}(\mathbf{n}-\mathbf{1})) + \mathbf{b}_h) \tag{3.3}$$
$$\mathbf{h}(\mathbf{n}) = (1 - \mathbf{z}(\mathbf{n})) \otimes \mathbf{h}(\mathbf{n}-\mathbf{1}) + \mathbf{z}(\mathbf{n}) \otimes \mathbf{h}(\mathbf{n}) \tag{3.4}$$
$$\mathbf{g}(\mathbf{n}) = \sigma(\mathbf{W}_n\mathbf{Feat}(\mathbf{n}) + \mathbf{b}_n) \tag{3.5}$$
$$\mathbf{u}(\mathbf{n}) = \mathbf{g}(\mathbf{n}) \otimes \mathbf{z}(\mathbf{n}) \tag{3.6}$$
$$\mathbf{out}(\mathbf{n}) = \mathbf{W}_{fc}\mathbf{u}(\mathbf{n}) + \mathbf{b}_{fc} \tag{3.7}$$

3.2.3. Complexity of SGRU with Offline Normalized Feature Extraction

Assume that the hidden size of SGRU is H. Therefore:

$$\begin{cases} Parameters\,in\,\mathbf{z}(\mathbf{n})\,layer & : 4 \times H + H \\ Parameters\,in\,\mathbf{r}(\mathbf{n})\,layer & : 4 \times H + H \\ Parameters\,in\,\mathbf{h}(\mathbf{n}-\mathbf{1})\,layer & : 4 \times H + H \times H + H \\ Parameters\,in\,\mathbf{g}(\mathbf{n})\,layer & : 4 \times H + H \\ Parameters\,in\,\mathbf{out}\,layer & : 2 \times H + 2 \end{cases} \tag{3.8}$$

Finally, the number of real-valued parameters in H-hidden SGRU is $22 \times H + H^2 + 2$.

3.3. Feature Engineering

Feature extraction is one of the most important factors determining the performance of NN-based DPD. Now NN-based DPD uses two types of feature extraction: offline feature extraction and online feature extraction. Offline feature extraction means the system calculates the chosen feature set and gives them to DPD as input. Offline feature selection mainly depends on the known characteristics of RF PA systems. For example, NN-based DPD firstly uses the ordinary and standard real-value inputs $I(n)$ and $Q(n)$ [15]. Then according to the nonlinearity characteristic, amplitude and phase are also applied [3] [18]. Based on GMP model, higher power order amplitude is chosen to augment the architecture [16][18]. To summary, wildly used offline features are $I(n), Q(n), |x(n)|^k (k = 1, 2, 3...), cos\theta(n), sin\theta(n)$. Conversely, online feature extraction directly passes basic features to a feature extraction NN layer. The feature extraction layer will output suitable input features automatically with the help of AI techniques [1] [2].

According to the comparison in Sec. 2.7, online feature extraction architecture performs over the off-line feature extraction. However, the online feature extraction layer in PG-JANET and DVR-JANET add barriers to hardware design.

Our work finally chose $|x(n)|^2$ to alternate $|x(n)|$ because it can avoid a square root operation. For phase perspective, $\theta(n)$ is the alternation pairs $sin\theta(n), cos\theta(n)$ to eliminate trigonometric and inverse trigonometric functions. $I(n)$ and $Q(n)$ are kept because they are important for improving of EVM. Therefore, the final set of characteristics is $I(n), Q(n), |x(n)|^2, \theta(n)$.

4

Experimental Results

In this Chapter, we validate the proposed SGRU model and E2E learning architecture on four different experimental validation platforms. Section 4.1 offers the validation foundation on simulated MATLAB platform. Section 4.2 shows the results on an online platform named RF WebLab, which can help researchers control the variables of the experiment and get relatively fair results. Section 4.3 and Section 4.4 exhibit the results on commercial Class-AB and Doherty PA.

4.1. Matlab Simulated Validation Platform

Before validation on real PA, simulated PA is a validation fundamental. If the new proposed DPD architecture cannot work on a simple simulation validation platform, getting a good result on a physical validation platform is impossible. This chapter shows validation experiment results from the MATLAB simulation platform. The results in this section show that:

1. The effectiveness of E2E learning architecture.

2. SGRU architecture is able to deal with the wideband OFDM signal distortion.

4.1.1. Experimental Setup

The simulation validation platform uses a 5×5 GMP matrix PA model operated at 3.7 GHz. The test signal is a 100 MHz OFDM-like signal with PAPR sampled at 860 MHz. This 64-QAM type modulation 100 MHz OFDM signal has 4096 subcarriers, 440 length guardbands, and 288 length cyclic prefix. The MATLAB simulated validation architecture is shown in Figure 4.1.

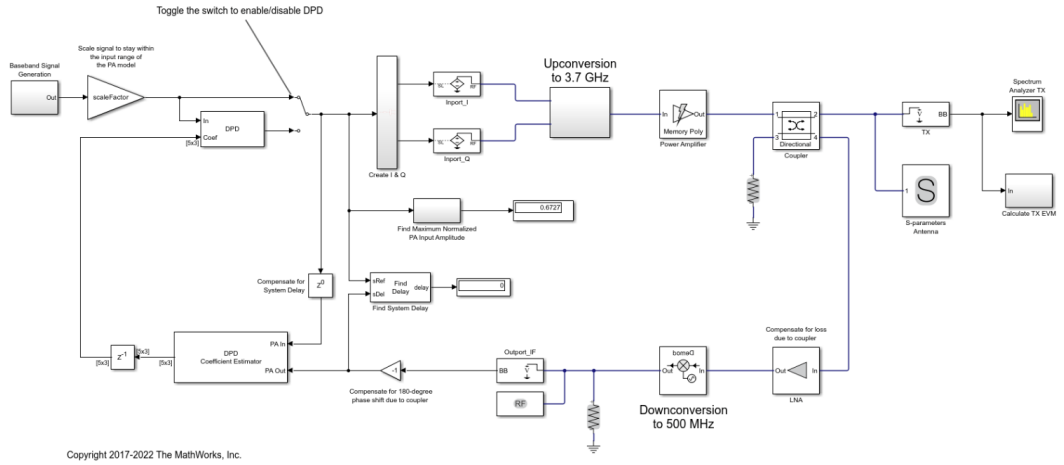

Figure 4.1: Block diagram of MATLAB simulated DPD validation platform.

180000 samples with 40 batch sizes are used for this simulated experiment. Unless otherwise mentioned, the data set is always divided into training, test, and validation sets according to the ratio of $14:3:3$. The first step, "training," uses $7/10$ of data. The training step uses the sequence-to-sequence regression mode shown in Figure 2.12. After calculating MSE loss and backpropagation, the ADAM optimization algorithm [33] helps to find the optimal parameters. Both the validation and the test steps use the NMSE Function 2.1 as their evaluation function. The learning rate uses a mode of stepping-decreasing adjustment as the validation results change. The initial value of the learning rate is 5×10^{-4}.

4.1.2. Experimental Results

We show the time-domain comparison results of PA modeling in 4.2. This result is generated from SGRU model with nine hidden neurons and 110 frame length. The PA modeling NMSE shown in the Figure is -30.42. It is observed that the predicted signal is very close to the ground truth signal from any perspective. With this PA NN model, we trained a DPD model with the same configuration. The DPD NMSE is -46.54. With this convergence precision, we obtained the lower band ACPR as -36.09 and the upper band ACPR as -36.65. The PA ACPR without DPD is $-28.92/28.54\,(lower/upper)$. The ACPR before and after DPD are collected with an output power of $40\,dBm$.

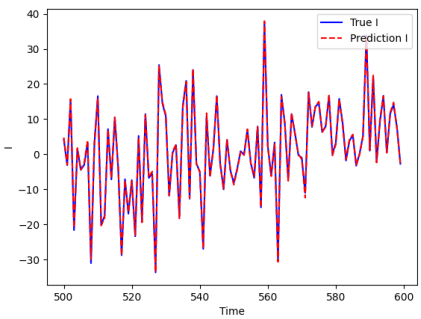

(a) Comparison between predicted I and true I.

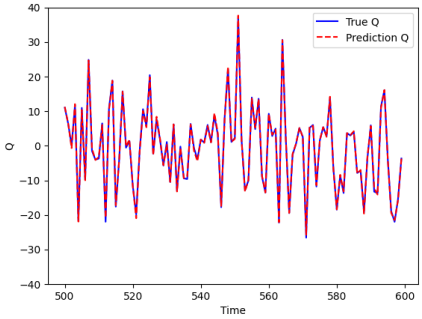

(b) Comparison between predicted Q and true Q.

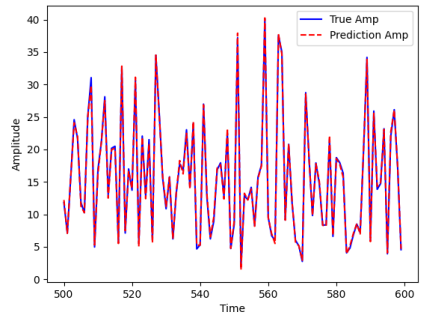

(c) Comparison between predicted amplitude and true amplitude.

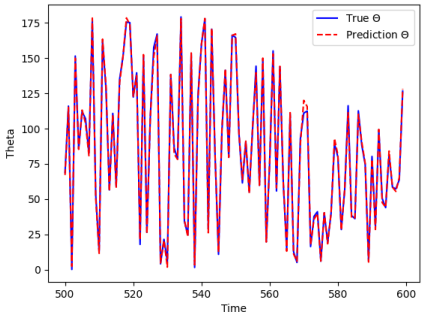

(d) Comparison between predicted phase and true phase.

Figure 4.2: Time domain comparison of PA modeling prediction and true signals.

4.2. RFWebLab Online Validation Platform

After validating on the MATLAB simulated platform, we came to a more practical and convenient environment, RF WebLab online measurement platform. In practical cases, the modulation mode, the PA nonlinear characteristic, and the measurement instrument noise can all be the reason that generates different performance results. One public measurement resource

is a good choice when we want to control variables between different works. There, the RF WebLab online RF PA measurement platform at Chalmers University is a good choice.

The experimental results in this section show that the SGRU can work as well as or even better than other complex DPD architectures with roughly the same number of parameters and easier operation.

4.2.1. Experimental Setup

RF WebLab measurement platform uses PXI chassis embedded PC accept, feedback data, and control measurement instruments. A Vector Signal Transceiver (PXIe-5646R VST) is used to up-convert the baseband signal to 2.14 GHz and down-converted 2.14 GHz signal to the baseband. The up-converted signal is passed to a linear driver amplifier, a GaN PA DUT, and a 30dB RF attenuator and then fed back to the VST. A MATLAB function helps customers to upload and download data pairs at the 200 MHz sampling rate. The first test signal is a 64-QAM modulation 50 MHz OFDM-like signal with 11.2 dB PAPR generated with 2048 subcarriers, 121 length guardbands and no cyclic prefix. The second test signal is a 64-QAM modulation 10 MHz OFDM-like signal with 11.2 dB PAPR generated with 64 subcarriers, 6 length guardbands, and without cyclic prefix. One million data samples are saved for each NN training. The architecture of RF WebLab validation platform is shown in Figure 4.3.

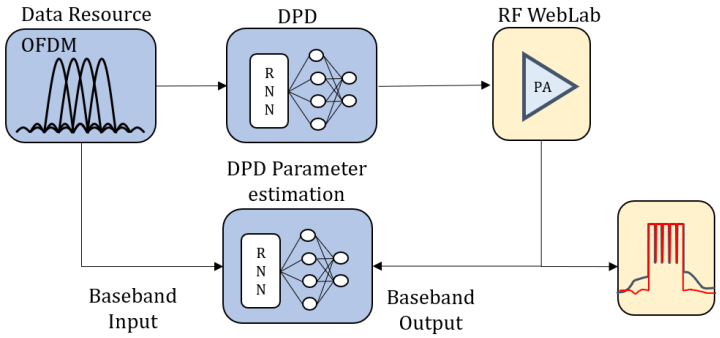

Figure 4.3: RF WebLab validation platform architecture.

1000000 data samples are used for each test. During model training, the data set is split into training, test and validation sets according to the $8:1:1$ ratio. The training criterion is NMSE and the optimizer is ADAM. The learning rate starts from $5e-4$ to decrease following the criterion.

4.2.2. Experimental Results

In this experiment, we compare the GMP, VDLSTM, DVR-JANET, PG-JANET and SGRU when each model has parameters around 150. The results are shown in Table 4.1.

Model Type	NMSE (dB)	ACPR (dBc) (lower/upper)	Number of Parameters (real-valued)
Without DPD	-33.84	-33.24/-32.57	N/A
GMP [34]	-48.51	-38.09/-37.32	150
VDLSTM [3]	-50.07	-38.81/-37.65	182
PG-JANET [1]	-44.71	-37.97/-37.77	154
CNN [32]	N/A	average -33.92 to -38.88	N/A
SGRU (Ours)	**-52.74**	**-38.49/-38.12**	**150**

Table 4.1: Performance Comparison of Different Architectures for the 50 MHz OFDM Signal

Table 4.1 shows that the SGRU model achieves the best NMSE and ACPR results. The ACPR performance keeps consistent with their NMSE performance. Based on this consistency, we can conclude that the PA model is close enough to the real PA with PA modeling NMSE of -33.84.

Sikp path structure comparison

According to papers [6] and [12], the skip path can help the RNN to focus on the nonlinear characteristics of RF PA. Based on this idea, we try to add a skip path to cover the non-linear trend except the memory effect so that the RNN can utilize most of the modeling capability on the memory effect. This subsection shows the verification results of three different skip path structures.

The SGRU architecture without skip path has a classic fully connected output layer as:

$$\mathbf{out}(\mathbf{n}) = \mathbf{W}_{fc}(\mathbf{h}(\mathbf{n}) + \mathbf{b}_{fc} \tag{4.1}$$

For the proposed SGRU architecture, the output layer is:

$$\begin{cases} \mathbf{g}(\mathbf{n}) & = \sigma(\mathbf{W}_n\mathbf{Feat}(\mathbf{n}) + \mathbf{b}_n) \\ \mathbf{out}(\mathbf{n}) & = \mathbf{W}_{fc}(\mathbf{g}(\mathbf{n}) \otimes \mathbf{z}(\mathbf{n})) + \mathbf{b}_{fc} \end{cases} \tag{4.2}$$

The skip path also has another location to add, which is to concatenate the input features and hidden neurons to control the skip path:

$$\begin{cases} \mathbf{g}(\mathbf{n}) & = \sigma(\mathbf{W}_n[\mathbf{Feat}(\mathbf{n}), \mathbf{h}(\mathbf{n})] + \mathbf{b}_n) \\ \mathbf{out}(\mathbf{n}) & = \mathbf{W}_{fc}(\mathbf{g}(\mathbf{n}) \otimes \mathbf{z}(\mathbf{n})) + \mathbf{b}_{fc} \end{cases} \tag{4.3}$$

In the schematic, these three structures are shown in Figure 4.4. The black path connecting input features and hidden neuron of RNN cell refers to Equation 4.2. Equation 4.3 is the red skip path shown in Figure 4.4.

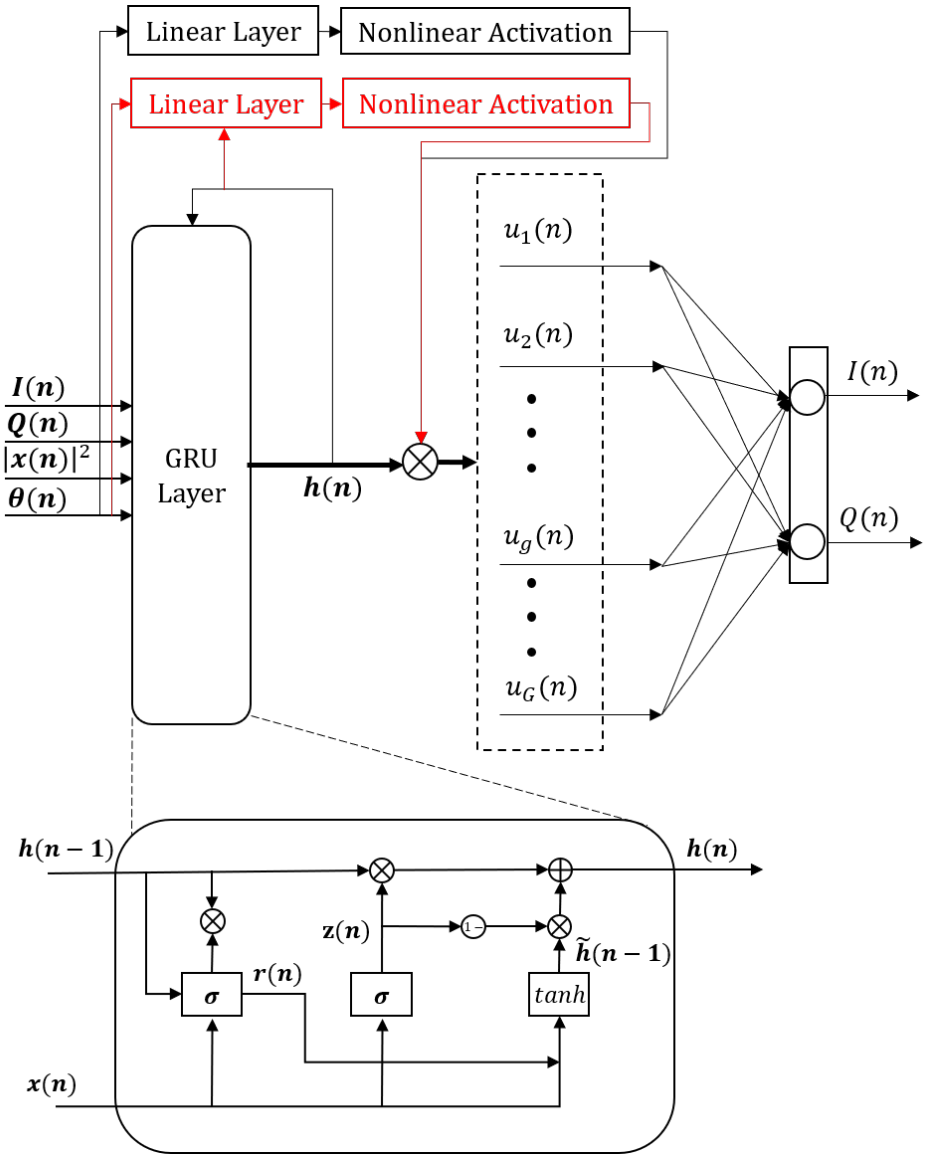

Figure 4.4: Schematic of different GRU models. The black skip path refers to Equation 4.2. The red skip path refers to Equation 4.3.

The NMSE and ACPR results are shown in Table 4.2. The result of the feature-controlled skip path (Function 4.2) shows the best average ACPR. Even if this kind of skip path decreases the lower band ACPR, it achieves balanced results while improving the lower and upper band ACPR.

Model Type	NMSE (dB)	ACPR (dBc) (lower/upper)	Number of Parameters (real-valued)
Without DPD	-33.84	-33.24/-33.57	N/A
GRU	-52.90	-39.02/-37.59	354
SGRU(Equation 4.2)	-52.09	-38.82/-38.05	368
SGRU(Equation 4.3)	-50.72	-38.91/-37.74	426

Table 4.2: Performance Comparison of GRU Architectures with different skip paths.

4.3. Commercial Class-AB Testboard

This section shows the DPD performance of wideband signal on the other Class-AB test board PA used in the RF WebLab platform. Compared to RF WebLab online platform, this chapter mainly works on the following:

1. This section shows the comparison between the proposed SGRU model and four different DPD architectures under 100 MHz and 200 MHz OFDM signals on Class-AB RF PA.
2. This section clarifies the details during the commercial measurement and instrument DPD validation platform setting up and data collection.

4.3.1. Experimental Setup

The commercial instrument validation platform consists of a test computer (PC), an Arbitrary Waveform Generator (Keysignt M8190A), a linear driver amplifier, a Doherty PA test board (CGH40006s-AMP1), -30dB RF attenuators, and a Signal and spectrum analyzer (FSW8) from Rohde & Schwarz. The setup is shown in Figure 4.5.

Figure 4.5: Commercial instrument validation platform for a Class-AB RF PA.

During the experiment, PC first generates a digital OFDM-like baseband signal, samples it at $8GHz$, and upconverts it to the RF frequency 2 GHz. The up-converted signal is emitted from the arbitrary waveform generator. The signal then passes through the linear driver amplifier, the DUT, and a -30dB RF attenuator, then is fed to the spectrum analyzer. The measurements have been conducted with different test signals that are 1024-QAM modulation 100 and 200 MHz OFDM signals with a peak-to-average power ratio of 7.7 dB (PAPR). The channel bandwidth of the test signal is fixed at 20 MHz. Therefore, the 100 MHz signal has five channels, and the 200 MHz signal has ten channels. Each channel has 1024 subcarriers and 110 guardbands. 800000 samples were recorded for training with four times baseband bandwidth frequencies, 400M Hz and 800MHz, respectively. Other 200000 samples were used to test the ACPR. Before and after adding DPD, the output power of PA is 24 dBm. Unless otherwise mentioned, the learning rate uses a mode of stepping-decreasing adjustment as the validation results change. The initial value of the learning rate is 5×10^{-4}.

4.3.2. Experimental Results

According to the E2E learning architecture, we first train the PA model to find the most accurate digital model. Here, the final used fixed-parameter PA model is a SGRU with a hidden size of nine.

Measurement Results with 100 MHz OFDM Signal

This part shows results from a 100 MHz OFDM-like signal test signal. All NN based DPD architecture are cascade to this PA model for training. We swept parameters from around 150 to around 400. We train all NN configurations five times at each hidden size. The average simulated NMSE results in Figure 4.6. Figure 4.7 reflect the results of ACPR from the trained models that are most close to their average NMSE.

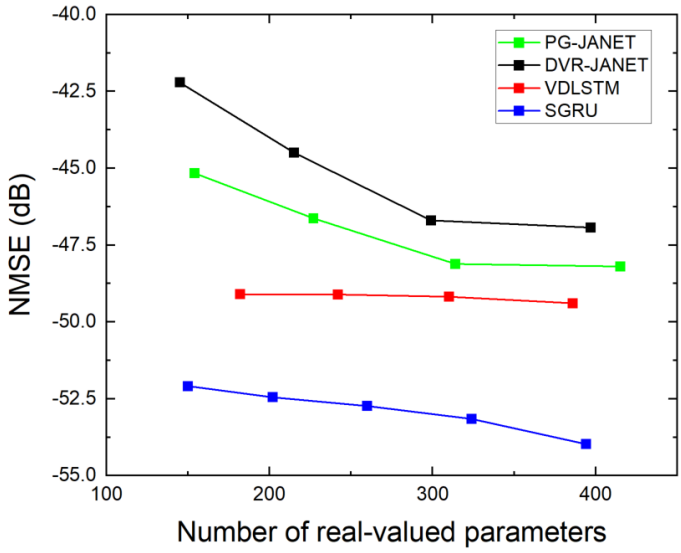

Figure 4.6: Simulated NMSE (dB) of the compared models for 100-MHz OFDM test of a Class-AB PA.

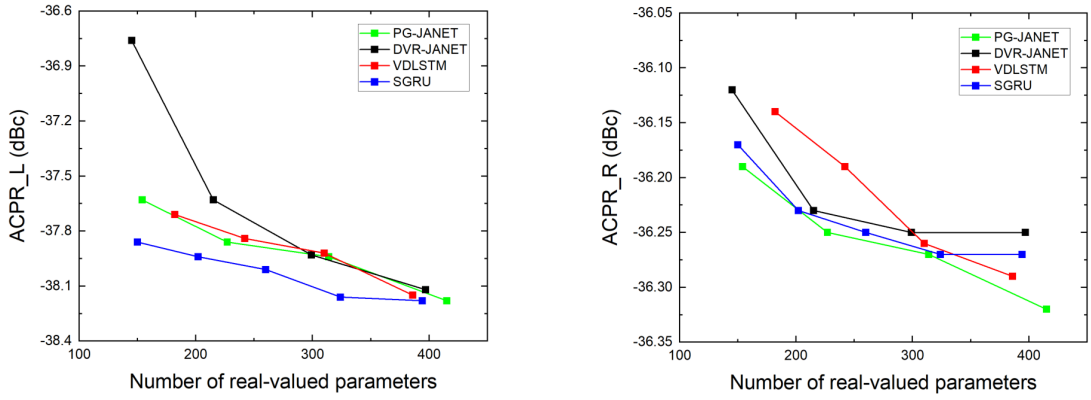

(a) ACPR (lower)

(b) ACPR (upper)

Figure 4.7: ACPR (dBc) of the compared models for 200-MHz OFDM test of a Class-AB PA.

The NMSE results show the capability of DPD NN to inverse the PA model. Here, the SGRU

offers a distinct convergence performance. The SGRU also shows the best average ACPR results at around 150 parameters. Table 4.3 digs into the results of these smallest parameters.

Model Type	NMSE (dB)	ACPR (dBc) (lower/upper)	Number of Parameters (real-valued)
Without DPD	-22.21	-32.4/-31.66	N/A
GMP [34]	-49.51±0.05	-36.53/-36.04	150
VDLSTM [3]	-49.10±0.28	-37.71/-36.14	182
PG-JANET [1]	-45.16±2.16	-37.63/-36.19	154
DVR-JANET [2]	-42.21±3.12	-36.67/-36.12	145
SGRU (Ours)	**-52.09±0.11**	**-37.86/-36.17**	**150**

Table 4.3: Performance Comparison of Different Architectures for the 100M Hz OFDM Signal

In Table 4.3, the ”without DPD NMSE” result is the PA modeling NMSE results. PG-JANET, DVR-JANET and SGRU are test with hidden size of 4. The VDLSTM is tested with the hidden size of 5. The GMP model uses the first two terms shown in Function 2.3 with a memory depth of 6 and a degree of 5. From the NMSE results, we can find that the GRU and LSTM models are more stable from training to training. For different PA and customers, it's easier to rebuild the outcome of these two configurations. The SGRU and PG-JANET results are competitive for ACPR.

Measurement Results with 200 MHz OFDM Signal

To validate the DPD capability with wider bandwidth, We also test the proposed architecture under 200 MHz OFDM-like signal test signal. Being similar to the 100 MHz experiments, We swept parameters from around 150 to around 400 and trained all the NN configurations five times at each hidden size. Figure 4.8 shows simulated NMSE results. Figure 4.9 reflects the results of ACPR from the trained models that are most close to their average NMSE.

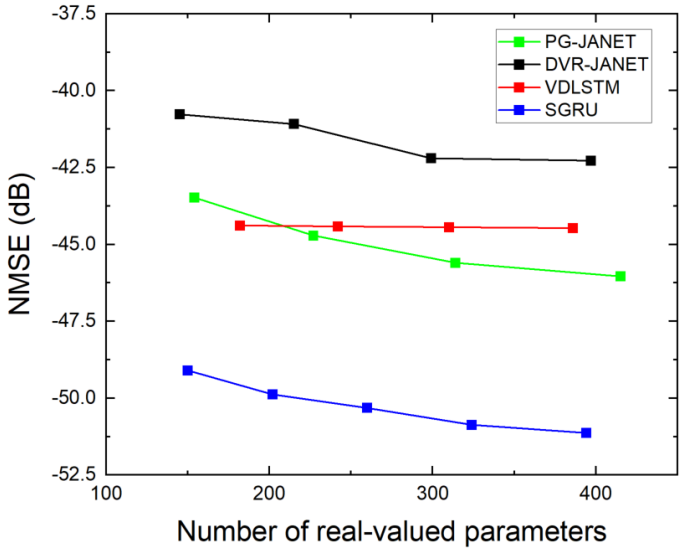

Figure 4.8: Simulated NMSE (dB) of the compared models for 200-MHz OFDM test of a Class-AB PA.

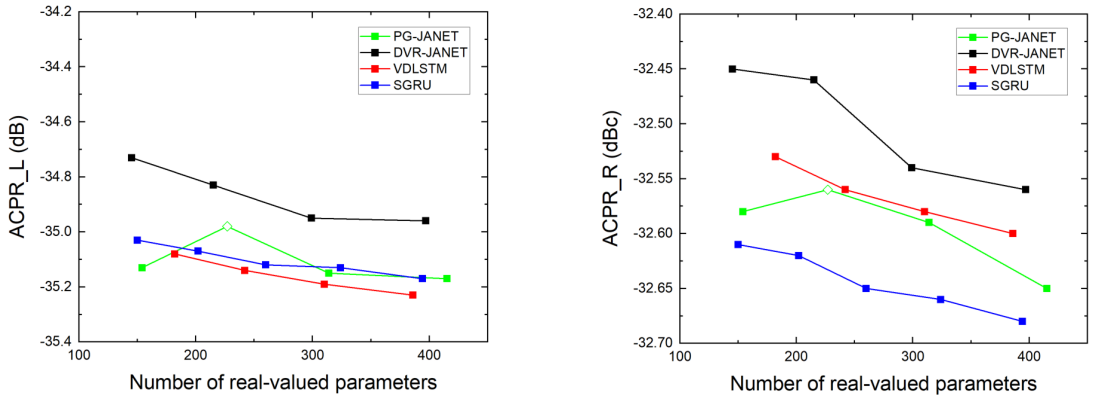

(a) ACPR (lower)

(b) ACPR (upper)

Figure 4.9: ACPR (dBc) of the compared models for 200-MHz OFDM test of a Class-AB PA.

From NMSE and ACPR trend Figures, we can verify that SGRU is still competitive among before state-of-art DPD configurations. The special red point on the line of PG-JANET reveals the problem caused by the unstable training process. For the proposed E2E learning architecture, the large NMSE standard deviation can cause outliers in the performance of ACPR. To clarify further, Table 4.4 specifies the details of the results with parameters around 150.

Model Type	NMSE (dB)	ACPR (dBc) (lower/upper)	Number of Parameters (real-valued)
Without DPD	-18.52	-31.98/-30.59	N/A
GMP [34]	-49.29±0.04	-34.25/-31.74	150
VDLSTM [3]	-44.41±0.06	-35.16/-32.58	182
PG-JANET [1]	-44.71±0.58	-34.68/-32.64	154
DVR-JANET [2]	-41.09±0.46	-34.73/-32.45	145
SGRU(Ours)	**-49.88±0.10**	**-35.03/-32.71**	**150**

Table 4.4: Performance Comparison of Different Architectures for the 200 MHz OFDM Signal on a Class-AB PA.

In Table 4.4, the configuration PG-JANET has the highest standard deviation. This means that the practical results will fluctuate more wildly than other NN architectures. The proposed SGRU got better upper band ACPR compared to VDLSTM while its' lower band ACPR is a little lower. It is worth noting that under the simple AMAM and AMPM characteristic, GMP exhibits outstanding capabilities in the wideband DPD of Class-AB compared to the results previously shown in Doherty. However, since the difference in the results of ACPR is very small, we still found that SGRU is quite competitive at least.

4.4. Commercial Doherty Testboard

In the last part of our experiment, we finally come to Doherty PA, which is used as a standard in previous works. Compared to the online Class-AB platform, this section mainly works on:

1. The new training process and performance with data normalization.
2. The influence of training frame length.
3. The EVM performance with proposed DPD architecture.

4. The proposed SGRU model has competitive performance and simpler architecture compared with four different DPD architectures under wideband 100 MHz and 200 MHz on Doherty RF PA.

4.4.1. Experimental Setup

The Doherty validation platform consists of a test computer (PC), an Arbitrary Waveform Generator (Keysignt M8190A), a linear driver amplifier (Amplifier Researcher Model 10S1G4A), a Doherty PA test board (Ampleon C5H38110AX), -40dB RF attenuators, and a Signal and spectrum analyzer (FSW8) from Rohde & Schwarz. The setup is shown in Figure 4.10.

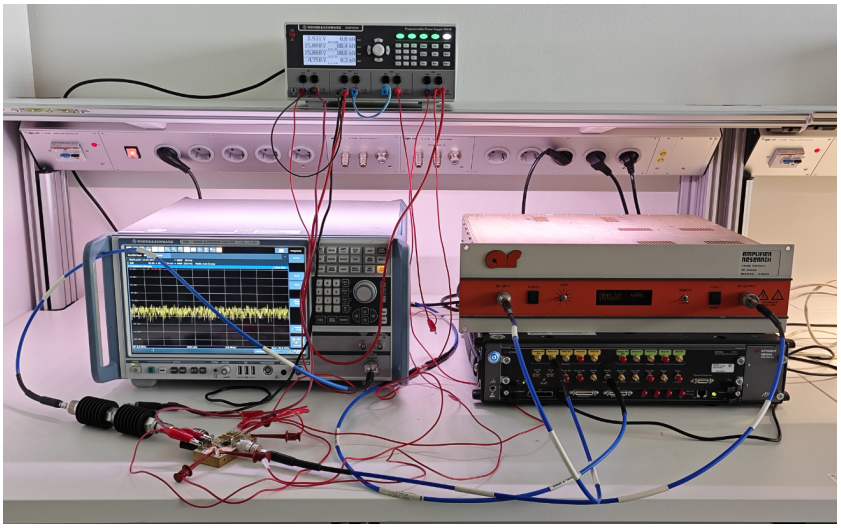

Figure 4.10: Commercial instrument validation platform for Doherty PA.

This experiment is based on 100 and 200 MHz OFDM-like signals. Both signals use 20 MHz for one channel. Each channel is encoded with 16-QAM, 1024 subcarriers, and 60 subcarriers as a guard band. To cooperate with the working characteristics of the PA and show the maximum effect of DPD as much as possible, we made a clip on the signal in the time domain. Naturally generated OFDM signals in our setup have PAPR greater than $10\,dB$, while we reduced it to around $7.5\,dB$. This can make the distribution of the OFDM signal more uniform, allowing the region where the gain is close to saturation to be fully reflected. However, this approach also improves the EVM around $1\,dB$ before processing. A better EVM makes the signal easier to handle than a completely naturally generated signal.

The OFDM signal is sampled at 8 GHz and then up-converted to 3.5 GHz in MATLAB. The signal generator passes the RF signal to the linear driver amplifier, the Doherty PA, and the $-40\,dB$ attenuator. The spectrum analyzer reads and analyzes the signal and feedback output signal in IQ format. Before and after adding DPD, the output power of PA is $39\,dBm$.

In the training, validation, and test process, 200000 samples were recorded for training with $400\,MHz$ for $100\,MHz$ signal and $800\,MHz$ for $200\,MHz$ signal. Other 50000 samples were used to test the ACPR and EVM. Unless otherwise mentioned, the learning rate uses a mode of stepping-decreasing adjustment from 5×10^{-4}.

4.4.2. Experimental Results

In this subsection, we first emphasize the special process of Doherty training. That is, all the data used are normalized data. In combination with the normalization process, we clarify a new training process. In the second part, we show how an important parameter of the training process, Frame Length, is determined. In the third and fourth sections, we show results based

on 100MHz and 200MHz OFDM signals. According to the E2E learning architecture, we first train the PA model to find the most accurate digital model. Here, the final used fixed-parameter PA model is a SGRU with a hidden size of 32, DVR-JANET with a hidden size of 23, PG-JANET with a hidden size of 23, VDLSTM with a hidden size of 29. All of them have parameters around 4000 and are trained with 100 epochs.

Data Normalization

In our proposed NN architecture, the features want to consider the I/Q imbalance and the amplitude/phase imbalance at the same time, so $I(n)$, $Q(n)$, $|x(n)|$, $\theta(n)$ are used as parallel features in the input layer. However, the range and distribution of these four features are different. The variance in Feature range will cause NN to attach different importance to them. The different distribution may lead to differences in the speed and effect of training, especially the distribution of θ. To reduce the impact of range and distribution on performance, we normalized both input and output data. After normalization, for training data pairs whose EVM is about $20\,dB$, the PA modeling NMSE can increase by $1\,dB$. And for training pairs whose EVM is about $24\,dB$, simulated NMSE can still improve by $0.1\,dB$. The specific training process is shown in Figure 4.11.

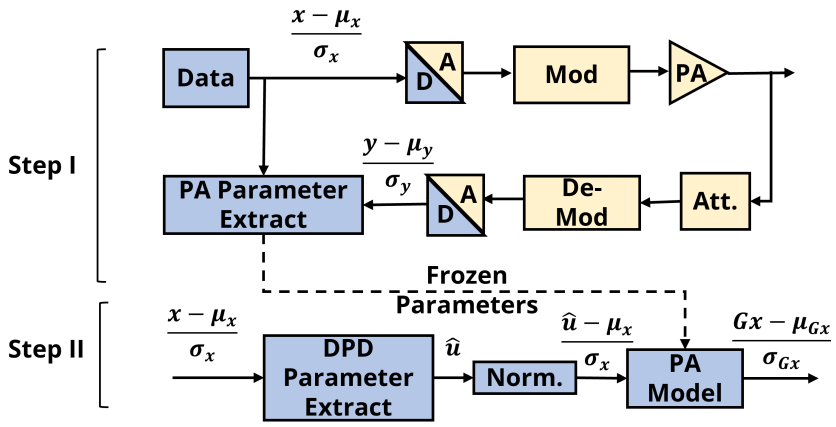

Figure 4.11: The training process with normalized data.

In the first training step, we directly change the training data pair to normalized input and output. However, in the second step, because the DPD better generates the ideal input without post-processing, we need to add a normalization step between the DPD model and the PA model. In this normalization block, we assume that the distribution of the ideal input u is close to the input x.

Frame Length Influence

The frame length is defined as the length of the time step in regression. This value may significantly affect the test results. In order to test the influence of frame length on the training results, we did a cross-validation for hidden size and frame length in the process of PA modeling. The total amount of data used by the model for training is controlled by adjusting the total number of epochs in the process. The Table 4.5 .

		Hidden size			
#epochs	**Frame length**	4	8	16	32
480	10	-34.492	-34.848	-34.935	-34.985
240	20	-34.126	-34.888	-34.967	-34.98
120	40	-34.261	-34.83	-34.971	-34.98
60	80	-34.596	-34.892	-34.954	-34.98
30	160	-34.482	-34.835	-34.925	-34.957

Table 4.5: The NMSE (dB) of training frame length in PA modeling.

The unstable results of hidden sizes 4 and 8 show that the small hidden size limits the influence of the frame length. When the hidden size is 32, the NN modeling capability is close to the maximum. The frame length of 10 offers the best results.

Mearsurement results with 100 MHz OFDM Signal

This part shows results based on 100 MHz OFDM-like signal test signal. The number of swept parameters starts from around 150 to around 2500. All the NN configurations five times at each hidden size to show the stability of different architecture.

Table A.1 shows the performance of the proposed SGRU architecture. In this table, 150 parameter results validate the modeling ability of SGRU with a very small number of parameters. Average ACPR, NMSE and EVM performance of 150 parameter are only $1.4\,dB$, $0.59\,dB$ and $0.51\,dB$ worse than the 2330 parameters. In addition, SGRU is a relatively stable architecture because most of the standard deviation is smaller than 0.2. This means that we can achieve fast retraining to achieve good performance when the system is adjusted.

Table A.2 offers the performance of DVR-JANET. To keep the setup consistent with the set-up of paper [2], the amplitude is considered as three segments. DVR-JANET in this experiment shows a gap between the smallest number of parameter results and other results. The DVR-JANET shows a better ability to deal with in-band nonlinearity and a weaker ability to deal with out-of-band nonlinearity. Moreover, DVR-JANET has more imbalance between the lower adjacent channel and the upper adjacent channel. For stability, the DVR-JANET model with 145 and 397 parameters have a large ACPR standard deviation compared to the SGRU model.

Table A.3 is the summary of PG-JANET performance results. PG-JANET has the worst performance with parameters around 150. Increasing the number of parameters of PG-JANET can improve performance mainly compared to other models. The parameter range that generates unstable results of PG-JANET is further expanded to the 530 parameters model. Due to instability, PG-JANET with 530 parameters even shows worse results than with 415 parameters.

VDLSTM achieve the best ACPR (lower) and the best EVM with a stable training process in this experiment, as shown in Table A.4. However, VDLSTM has two shortcomings in the results. The first one is the imbalance between the upper and lower adjacent channels. The second is that VDLSTM has overfitting with parameters larger than 1142. This means that performance cannot be improved more with increasing NN size.

To compress the number of parameters as much as possible, we choose SGRU with 394 parameters, DVR-JANET with 397 parameters PG-JANET with 415 parameters, and VDLSTM with 310 parameters to compare the specific value. The comparison is shown in Table 4.6. In the following, we refer to data in Table 4.6 as comparison points.

Model	NMSE (dB)	ACPR_L (dBc)	ACPR_R (dBc)	EVM (dB)	#params
w/o DPD	-34.98	-30.5	-28.89	-24.58	N/A
DVR-JANET [2]	-37.17±0.28	-45.04±0.92	-43.22±1.00	-37.70±0.26	397
PG-JANET [1]	-36.85±0.28	-44.52±0.92	-42.74±1.00	-37.62±0.26	415
VDLSTM [3]	**-37.33±0.14**	-45.97±0.25	-43.39±0.66	**-38.16±0.20**	310
SGRU (Ours)	-37.17±0.62	**-45.16±0.39**	**-44.31±0.21**	-37.72±0.15	394

Table 4.6: Performance comparison for 100 MHz OFDM signal.

Figure 4.12 shows the NMSE performance comparison. Here we found that NMSE and other performances are not consistent. This experiment also has not achieved NMSE better than $-40/, dB$, as shown in previous work. There are three reasons for this result. The first is that the equipment in the actual test is different from previous works. The noise of the equipment may make the NMSE less than $-40\,dB$ but still achieve very good ACPR and EVM performance. The second reason is that we choose the ideal amplification gain for calculating NMSE is chosen by ourselves, and the fluctuation of this value can also change the NMSE value. The third is because our performance without DPD is the first test result that embodies Doherty's gain compression. This means that when the target gain is constant, the result of NMSE will increase. It is worth mentioning that SGRU still achieves the best target gain, which is $0.1\,dB$ larger than the other three structures.

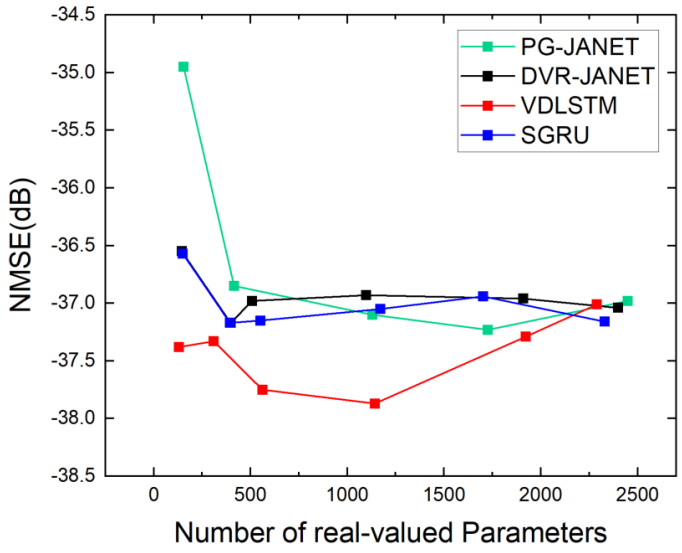

Figure 4.12: NMSE (dB) of the compared models for 100-MHz OFDM test of Doherty PA.

Figure 4.13 shows the ACPR performance comparison. At comparison points, four architectures improve ACPR by $15.04\,dB$, $14.96\,dB$, $13.85\,dB$, and $14.9\,dB$ on the order of SGRU, DVR-JANET, PG-JANET and DVR-JANET-JANET.

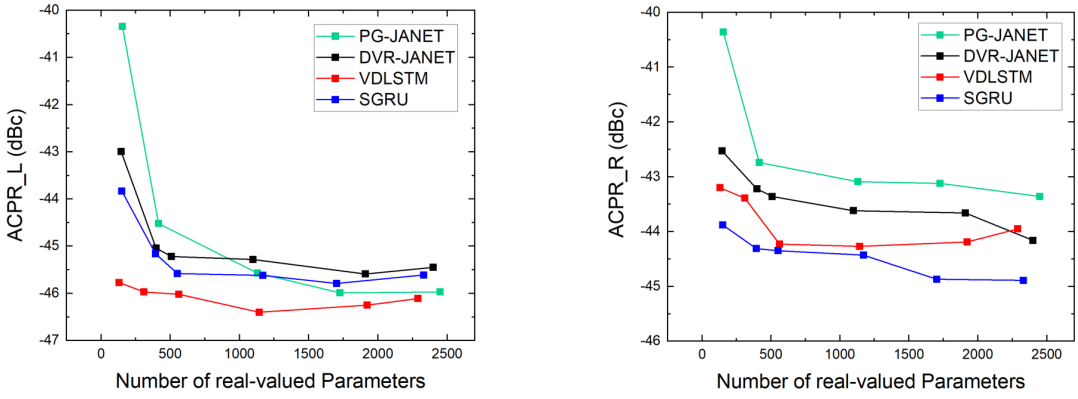

(a) ACPR (lower) **(b)** ACPR (upper)

Figure 4.13: ACPR (dBc) of the compared models for 100-MHz OFDM test of a Doherty PA.

Figure 2.2 is the EVM performance comparison. At the comparison point, SGRU still shows better performance than DVR-JANET and PG-JANET, while VDLSTM has the best EVM performance. The DPD can improve the EVM by around $14\,dB$

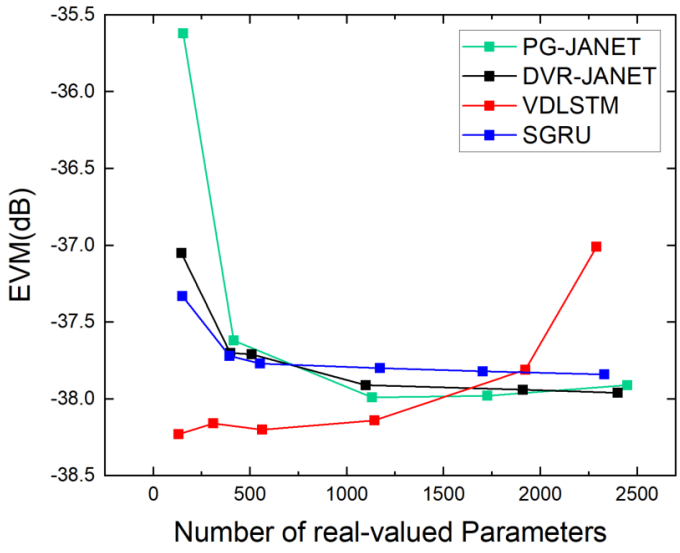

Figure 4.14: EVM(dB) of the compared models for 100-MHz OFDM test of a Doherty PA.

Figure 4.15 shows the AM/AM and AM/PM characteristics with and without DPD. The figure with DPD is generated from SGRU with 394 parameters.

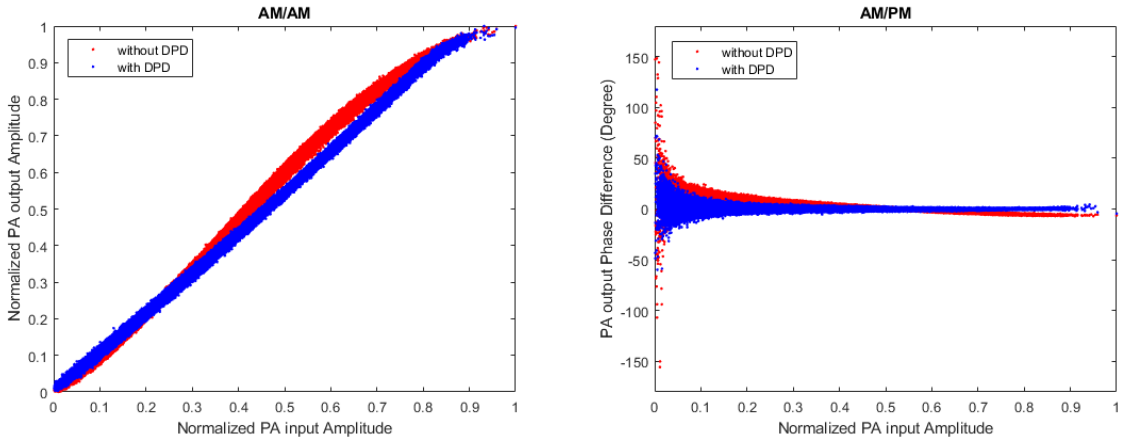

(a) Normalized Input Amplitude vs. Normalized Output Amplitude

(b) Normalized Input Amplitude vs. Phase difference between Input and Output

Figure 4.15: AM/AM and AM/PM with and without DPD.

Mearsurement results with 200 MHz OFDM Signal

For 200 MHz OFDM test, we also compare the architectures at the parameters shown in 4.7.

Model	NMSE (dB)	ACPR_L (dBc)	ACPR_R (dBc)	EVM (dB)	#params
w/o DPD	-23.73	-28.89	-29.86	-21.28	N/A
DVR-JANET [2]	-23.25±0.16	-33.95±0.11	-39.47±0.23	-23.88±0.10	397
PG-JANET [1]	-23.79±0.28	-37.60±0.47	-40.88±0.27	-24.03±0.03	415
VDLSTM [3]	-24.1±0.09	-38.33±0.30	-42.01±0.13	-24.21±0.05	310
SGRU (Ours)	-23.61±0.32	-37.85±0.44	-41.55±0.13	-24.09±0.07	394

Table 4.7: Performance comparison for 200 MHz OFDM signal.

In this table, it can be observed that the VDLSTM shows the best results. The proposed SGRU architecture shows close performance to VDLSTM. Comparing VDLSTM and SGRU, we tried three ways to improve the performance of SGRU architecture: replace the $|x|^2$ feature with $|x|$ feature, replace the θ feature with $cos(\theta), sin(\theta)$ features and replace the GRU kernel with LSTM kernel. The SGRU with $I, Q, |x|, \theta$ features finally works better. As shown in Table 4.8, SGRU improved the ACPR from $-28.89/-29.86\,dB$ to $-38.44/-42.09\,dB$ and decrease the EVM by $2.94dB$. For both upper and lower band, SGRU generated better ACPR with $I, Q, |x|, \theta$ features.

Model	NMSE (dB)	ACPR_L (dBc)	ACPR_R (dBc)	EVM (dB)	#params
VDLSTM [3]	-24.1	-38.33	-42.01	-24.21	310
SGRU (Ours)	-23.85	-38.44	-42.09	-24.22	394

Table 4.8: Performance comparison for VDLSTM and SGRU with amplitude as feature signal.

Figure 4.16 shows the AM/AM and AM/PM characteristics with and without DPD for 200 MHz. The figure with DPD is generated from SGRU with 394 parameters. Compared to 100 MHz test, we can observe that the memory effect after DPD still affect the performance a lot. However, in our experiment setup, the ACPR floor of input signal is only $-42\,dB$. With a better white noise condition, SGRU can generate a more clean AM/AM figure and better EVM.

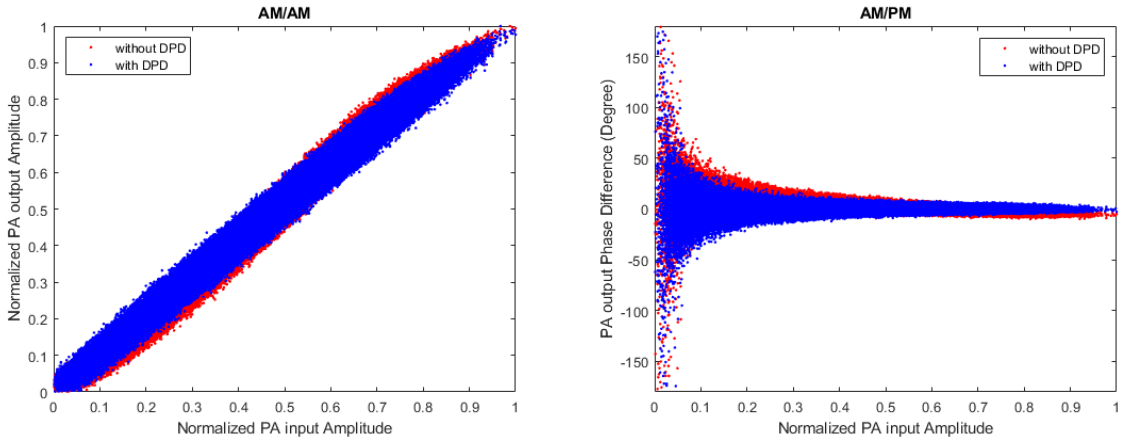

(a) Normalized Input Amplitude vs. Normalized Output Amplitude

(b) Normalized Input Amplitude vs. Phase difference between Input and Output

Figure 4.16: AM/AM and AM/PM with and without DPD.

The detailed results of the four structures tested on 200MHzOFDM signals are shown in Tables A.5, A.6, A.7, and A.8.

4.5. Discussion

This section further discusses the following issues revealed in the results.

1. Special data pre-processing for the RFWebLab online validation platform.
2. Analysis of the reasons for the difference from the previous works.
3. Analysis of the calculation complexity of different NN architecture.

4.5.1. Data preprocessing of RFWebLab

RF Weblab has fixed settings that customers cannot change. These settings reveal two problems when we collect wide-band data sets. Firstly, popular signal analyzers such as the FSW series from Rohde & Schwarz can only cancel their internal noise while testing power. When the signal analyzer feedback baseband output I and Q signal of PA, the noise can cause convergence problems under small signals. As shown in Figure 4.17, the red points are collected from the input signal without a modified input range. The fluctuation range of gain exceeds the normal range. Moreover, under normal encoding conditions, these sampling points represent a large proportion of the total sampling points. It's difficult for PA modeling NN to find accurate results with too much random noise.

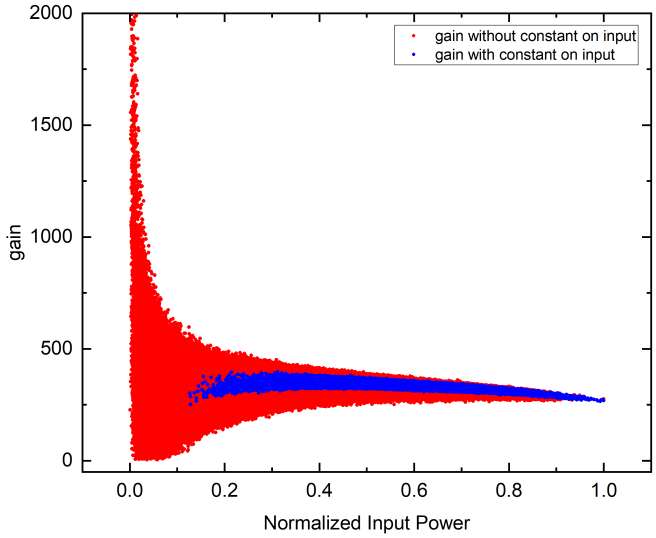

Figure 4.17: Gain vs Normalized input power with and without data preprocessing.

To solve this noise problem, two intuitive methods can be used. The first one is: Adding a filter to do denoise to close the collect signal to the actual signal. Here, we find the second problem. Under RF WebLab settings, we did not know the real ACPR of the signal at Radio Frequency. This unknown situation not only makes the denoising method hard to implement, but also causes the untrusted base band ACPR calculation results.

To avoid these two problems on the RF WebLab, we took a similar approach to improve the smallest input signal power as in Paper [32]. An in-band impulse is added to the frequency domain to add a constant to the time domain. The normalized power spectrum density before and after adding a constant is shown in Figure 4.18.

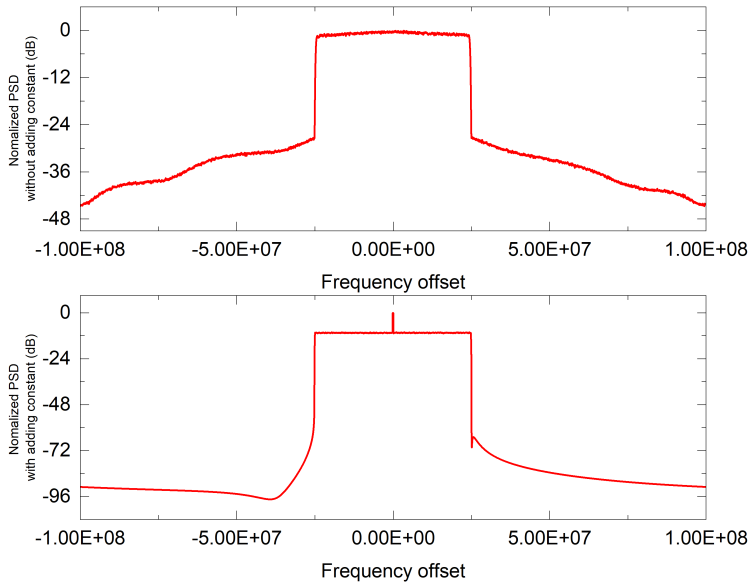

Figure 4.18: The normalized power spectrum density before and after adding a constant.

This impulse will change the center of the constellation plot but not the distribution. After adding this impulse, the data set became the blue points shown in Figure 4.17. Without any other changes, we can observe that the data became much more clean.

During the experiment, the PA modeling step got NMSE of around -19 from raw data while it got NMSE of around -33 from data with impulse.

4.5.2. Reasons Analysis for the Difference from the Previous Works

Although SGRU with $|x^2|$ are not the best architecture in the finished hidden swept experiment for 200 MHz OFDM test of Doherty PA, we can still find some important information from the results difference from previous works.

Figure 4.19 shows the ACPR performance for 200 MHz OFDM test of Doherty PA. Figure 4.20 shows the EVM performance for 200 MHz OFDM test of Doherty PA. DVR-JANET shows weak performance compared to other three architectures. This can be generated for two reasons: The first one is that we still use three amplitude threshold for DVR-JANET while paper [2] use five amplitude threshold for 200 MHz test. The second reason is that we choose the number of training epochs based on the convergence speed of SGRU, which is only 100. However, paper [1] used 750 training epochs, and paper [2] used 500 training epochs.

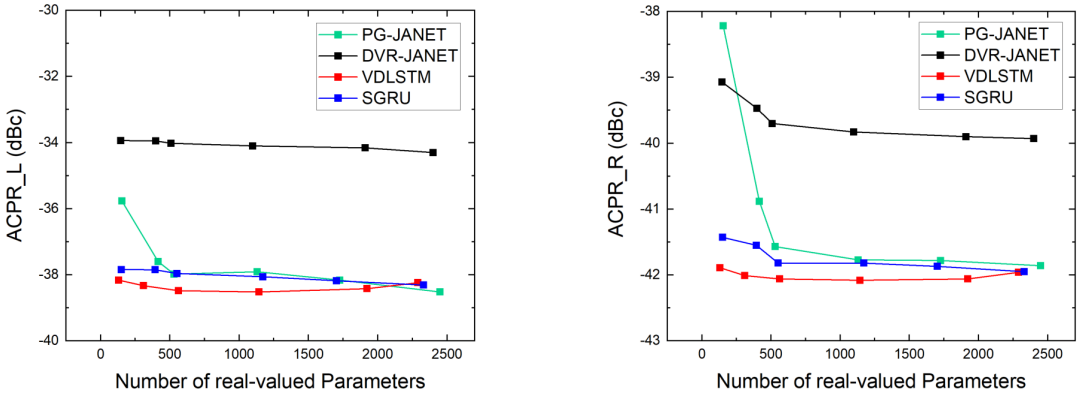

(a) ACPR (lower) **(b)** ACPR (upper)

Figure 4.19: ACPR (dBc) of the compared models for 200-MHz OFDM test of Doherty PA.

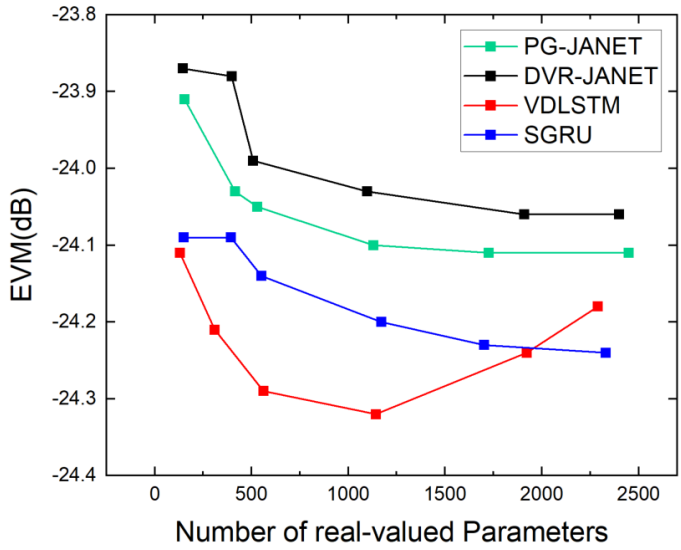

Figure 4.20: EVM(dB) of the compared models for 200-MHz OFDM test of Doherty PA.

4.5.3. Calculation Complexity Analysis

First, we plot the Power spectral density (PSD) under 100 and 200 MHz test signal of Class-AB PA in Figure 4.21. At the comparison points mentioned in 4.4.2, the normalized PSD is shown in Figure 4.22. We can observe that all NN architectures show close results compared to the PSD without DPD. The difference between the ACPR can't determine a significant advantage of any configuration. Therefore, we consider that all tested DPD models have similar pre-distortion ability in this experiment environment. At this point, the focus of our comparison shifts to the computational and practical difficulty of different architectures.

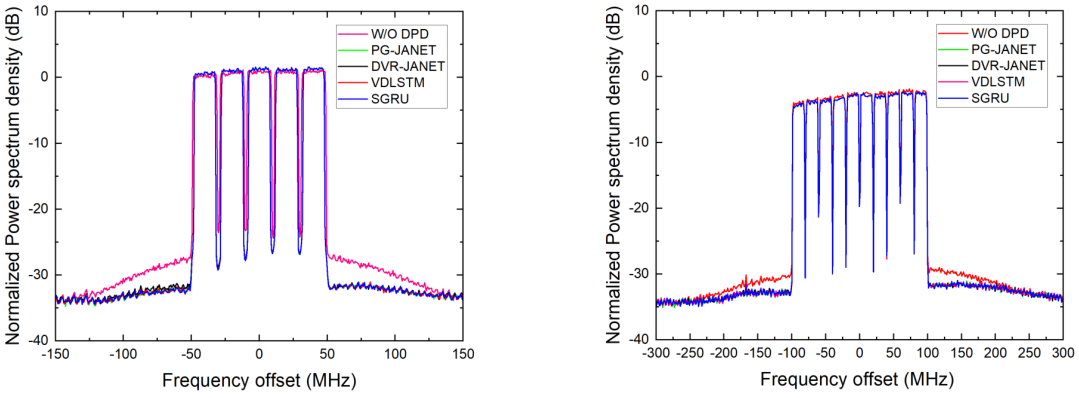

(a) 100 MHz **(b)** 200 MHz

Figure 4.21: Normalized Power Spectrum Density (dB) comparison on Class-AB PA.

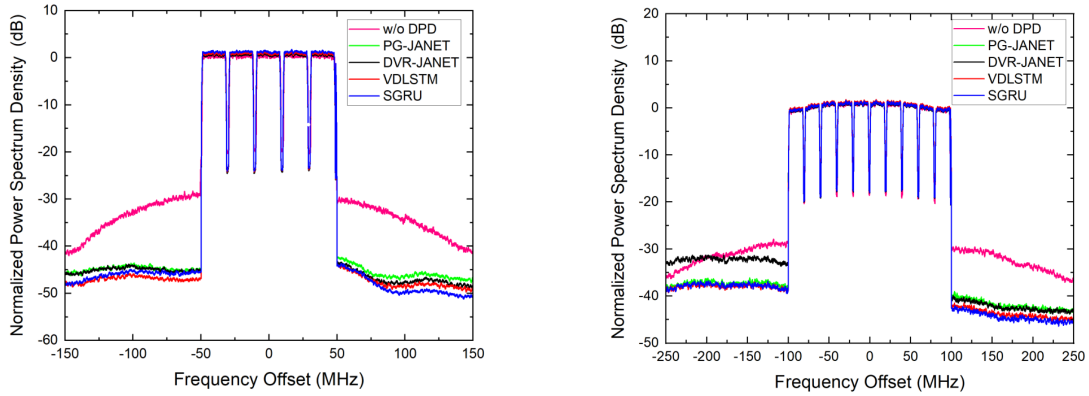

(a) 100 MHz **(b)** 200 MHz

Figure 4.22: Normalized Power Spectrum Density (dB) comparison on Doherty PA.

The practical difficulty for the GMP model is that the parameters are complex. Moreover, the input features in all configurations except SGRU need to calculate square root results for magnitude. VDLSTM, DVR-JANET and PG-JANET also need to calculate the cosine and sine value. These two features will add barriers to the hardware implementation of DPD. SGRU used alternative $|x(n)|^2, \theta(n)$ to skip both the square root and sine calculation. For this reason, the hardware implementation for SGRU is more positive than other architectures.

5

Conclusion, Limitation, and Outlook

5.1. Conlusion

After the analysis of the results, it can be concluded that the proposed methodology has competitive performance with previous state-of-art work.

1. The proposed SGRU can achieve a good out-of-band nonlinearity improvement of the wideband OFDM signal for both Class-AB and Doherty PA with smaller parameters. In section 4.3 and section 4.4, SGRU shows better improved ACPR than DVR-JANET and PG-JANET with parameters less than 400. Even if VDLSTM always offers the best lower adjacent channel ACPR, proposed SGRU is good at balancing upper and lower adjacent channels.

2. Proposed SGRU can improve the in-band linearity of Doherty a lot. In section 4.4, the proposed SGRU with 394 parameters improved the EVM by $13.2\,dB$ for 100MHz OFDM signal.

3. NMSE is not one of the ideal metrics. In the actual validation process, it is affected by many complex factors and cannot fully reflect the model's ability to deal with non-linearity. Therefore, the results of EVM should be provided as much as possible.

4. The E2E learning architecture greatly reduces the parameters required for AI-based DPD. In the process of PA modeling, the accuracy will increase with the increase in the number of parameters. However, in the final application, the PA model does not participate. Even if we use a large-size NN for PA modeling, small-size NNs can still calculate a relatively accurate inverse model for DPD application.

5.2. Limitations

There are still many deficiencies in our work. From the perspective of the experimental setup, due to the offset of the constellation in OFDM signal generation, the results shown in the class-AB section may not be our best results. In addition, we use $|x|^2$ instead of $|x|$ for the 200 MHz hidden size scan for the following reasons: 1. DVR-JANET is the previous state-of-the-art NN model for DPD. After we checked that SGRU performed better than DVR-JANET, we did the final test directly. 2. We made SGRU produce better results than VDLSTM at 100 MHz. 3. In Paper [1], VDLSTM has been verified to perform weaker than PG-JANET. In fact, different test platforms, different bandwidths, and even different OFDM signal settings are definitely likely to affect the final result. If we use SGRU, we should test different combinations of Features first. On the basis of the results of the feature test, the best combination of the test platform and

bandwidth can be selected. For the architecture design, the main limitation of this work is that the proposed SGRU's ability to improve EVM is not the best of all architectures.

5.3. Outlook

For the future of this work, there are several points to explore. The first is how to absorb the EVM improvement ability of VDLSTM and understand why the position in which phase information is added is so important for EVM. The second is about the process of using normalized data. We selected the same distribution parameters for the ideal input as the general input signal, but their distributions are not the same in practice. Exploring the influence of distribution parameters further may help to improve the performance of DPD. The third is whether we can make DPD handle more situations by adding other parameters, such as different PAPR or different loads.

For other feasible topics derived from this topic, reducing the PAPR of OFDM by AI method and keeping the constellation unchanged can be significant for the accuracy of signal demodulation.

For the whole system of RF PA, we found that the designers of Doherty PA are more concerned about the gain compression caused by the increase of input power. To make DPD able to handle the gain compression above $3\,dB$ is the work that DPD can cooperate with the designers of other components of the RF system. Finally, DPD may also be embedded in a multiway Doherty PA system.

References

[1] Tugce Kobal et al. “Digital Predistortion of RF Power Amplifiers With Phase-Gated Recurrent Neural Networks”. In: *IEEE Transactions on Microwave Theory and Techniques* 70.6 (2022), pp. 3291–3299. DOI: 10.1109/TMTT.2022.3161024.

[2] Tugce Kobal and Anding Zhu. “Digital Predistortion of RF Power Amplifiers With Decomposed Vector Rotation-Based Recurrent Neural Networks”. In: *IEEE Transactions on Microwave Theory and Techniques* 70.11 (2022), pp. 4900–4909. DOI: 10.1109/TMTT.2022.3209658.

[3] Hongmin Li et al. “Vector Decomposed Long Short-Term Memory Model for Behavioral Modeling and Digital Predistortion for Wideband RF Power Amplifiers”. In: *IEEE Access* 8 (2020), pp. 63780–63789. DOI: 10.1109/ACCESS.2020.2984682.

[4] P.B. Kenington. “Linearized transmitters: an enabling technology for software defined radio”. In: *IEEE Communications Magazine* 40.2 (2002), pp. 156–162. DOI: 10.1109/35.983923.

[5] Michael S . Heutmaker, Eleanor Wu, and John R. Welch. “Envelope Distortion Models with Memory Improve the Prediction of Spectral Regrowth for Some RF Amplifiers”. In: *48th ARFTG Conference Digest*. Vol. 30. 1996, pp. 10–15. DOI: 10.1109/ARFTG.1996.327183.

[6] Chance Tarver et al. “Neural Network DPD via Backpropagation through a Neural Network Model of the PA”. In: *2019 53rd Asilomar Conference on Signals, Systems, and Computers*. 2019, pp. 358–362. DOI: 10.1109/IEEECONF44664.2019.9048910.

[7] A. A. M. Saleh and J. Salz. “Adaptive linearization of power amplifiers in digital radio systems”. In: *The Bell System Technical Journal* 62.4 (1983), pp. 1019–1033. DOI: 10.1002/j.1538-7305.1983.tb03113.x.

[8] A.N. D’Andrea, V. Lottici, and R. Reggiannini. “Nonlinear predistortion of OFDM signals over frequency-selective fading channels”. In: *IEEE Transactions on Communications* 49.5 (2001), pp. 837–843. DOI: 10.1109/26.923807.

[9] H.N Mhaskar and Charles A Micchelli. “Approximation by superposition of sigmoidal and radial basis functions”. In: *Advances in Applied Mathematics* 13.3 (1992), pp. 350–373. ISSN: 0196-8858. DOI: https://doi.org/10.1016/0196-8858(92)90016-P.

[10] J. Wood, D.E. Root, and N.B. Tufillaro. “A behavioral modeling approach to nonlinear model-order reduction for RF/microwave ICs and systems”. In: *IEEE Transactions on Microwave Theory and Techniques* 52.9 (2004), pp. 2274–2284. DOI: 10.1109/TMTT.2004.834554.

[11] M. Ibnkahla et al. “Neural network modeling and identification of nonlinear channels with memory: algorithms, applications, and analytic models”. In: *IEEE Transactions on Signal Processing* 46.5 (1998), pp. 1208–1220. DOI: 10.1109/78.668784.

[12] Kaiming He et al. “Deep residual learning for image recognition”. In: *Proceedings of the IEEE conference on computer vision and pattern recognition*. 2016, pp. 770–778.

[13] M. Isaksson, D. Wisell, and D. Ronnow. “Wide-band dynamic modeling of power amplifiers using radial-basis function neural networks”. In: *IEEE Transactions on Microwave Theory and Techniques* 53.11 (2005), pp. 3422–3428. DOI: 10.1109/TMTT.2005.855742.

[14] I. Santamaría and M. Ibáñez J.and Lázaro. “Modeling Nonlinear Power Amplifiers in OFDM Systems from Subsampled Data: A Comparative Study Using Real Measurements”. In: *EURASIP Journal on Advances in Signal Processing* (2003). DOI: 10.1155/S1110865703306067.

[15] Praveen Jaraut, Meenakshi Rawat, and Fadhel M. Ghannouchi. “Composite Neural Network Digital Predistortion Model for Joint Mitigation of Crosstalk, I/Q Imbalance, Nonlinearity in MIMO Transmitters”. In: *IEEE Transactions on Microwave Theory and Techniques* 66.11 (2018), pp. 5011–5020. DOI: 10.1109/TMTT.2018.2869602.

[16] Dongming Wang et al. “Augmented Real-Valued Time-Delay Neural Network for Compensation of Distortions and Impairments in Wireless Transmitters”. In: *IEEE Transactions on Neural Networks and Learning Systems* 30.1 (2019), pp. 242–254. DOI: 10.1109/TNNLS.2018.2838039.

[17] Yibo Wu et al. “Residual Neural Networks for Digital Predistortion”. In: *GLOBECOM 2020 - 2020 IEEE Global Communications Conference*. 2020, pp. 01–06. DOI: 10.1109/GLOBECOM42002.2020.9322327.

[18] Yikang Zhang et al. “Vector Decomposition Based Time-Delay Neural Network Behavioral Model for Digital Predistortion of RF Power Amplifiers”. In: *IEEE Access* 7 (2019), pp. 91559–91568. DOI: 10.1109/ACCESS.2019.2927875.

[19] Danh Luongvinh and Youngwoo Kwon. “Behavioral modeling of power amplifiers using fully recurrent neural networks”. In: *IEEE MTT-S International Microwave Symposium Digest, 2005.* 2005, pp. 1979–1982. DOI: 10.1109/MWSYM.2005.1517131.

[20] Meenakshi Rawat, Karun Rawat, and Fadhel M. Ghannouchi. “Adaptive Digital Predistortion of Wireless Power Amplifiers/Transmitters Using Dynamic Real-Valued Focused Time-Delay Line Neural Networks”. In: *IEEE Transactions on Microwave Theory and Techniques* 58.1 (2010), pp. 95–104. DOI: 10.1109/TMTT.2009.2036334.

[21] Junyoung Chung et al. *Empirical Evaluation of Gated Recurrent Neural Networks on Sequence Modeling*. 2014. DOI: 10.48550/ARXIV.1412.3555. URL: https://arxiv.org/abs/1412.3555.

[22] Taijun Liu et al. “Digital Predistortion Linearization with Deep Neural Networks for 5G Power Amplifiers”. In: *2019 European Microwave Conference in Central Europe (EuMCE)*. 2019, pp. 216–219.

[23] Jinlong Sun et al. “Behavioral Modeling and Linearization of Wideband RF Power Amplifiers Using BiLSTM Networks for 5G Wireless Systems”. In: *IEEE Transactions on Vehicular Technology* 68.11 (2019), pp. 10348–10356. DOI: 10.1109/TVT.2019.2925562.

[24] Gang Li et al. “Instant Gated Recurrent Neural Network Behavioral Model for Digital Predistortion of RF Power Amplifiers”. In: *IEEE Access* 8 (2020), pp. 67474–67483. DOI: 10.1109/ACCESS.2020.2986816.

[25] Jos van der Westhuizen and Joan Lasenby. “The unreasonable effectiveness of the forget gate”. In: *CoRR* abs/1804.04849 (2018). arXiv: 1804.04849. URL: http://arxiv.org/abs/1804.04849.

[26] Xin Hu et al. “Convolutional Neural Network for Behavioral Modeling and Predistortion of Wideband Power Amplifiers”. In: *IEEE Transactions on Neural Networks and Learning Systems* 33.8 (2022), pp. 3923–3937. DOI: 10.1109/TNNLS.2021.3054867.

[27] Henna Paaso and Aarne Mammela. “Comparison of direct learning and indirect learning predistortion architectures”. In: *2008 IEEE International Symposium on Wireless Communication Systems*. 2008, pp. 309–313. DOI: 10.1109/ISWCS.2008.4726067.

[28] Fa-Long Luo, ed. *Digital front-end in wireless communications and broadcasting: circuits and signal processing*. Cambridge University Press, 2011.p257.

[29] Jessica Chani-Cahuana et al. “Iterative Learning Control for RF Power Amplifier Linearization”. In: *IEEE Transactions on Microwave Theory and Techniques* 64.9 (2016), pp. 2778–2789. DOI: 10.1109/TMTT.2016.2588483.

[30] Reina Hongyo et al. “Deep Neural Network-Based Digital Predistorter for Doherty Power Amplifiers”. In: *IEEE Microwave and Wireless Components Letters* 29.2 (2019), pp. 146–148. DOI: 10.1109/LMWC.2018.2888955.

[31] Deepmala Phartiyal and Meenakshi Rawat. “LSTM-Deep Neural Networks based Predistortion Linearizer for High Power Amplifiers”. In: *2019 National Conference on Communications (NCC)*. 2019, pp. 1–5. DOI: 10.1109/NCC.2019.8732178.

[32] Udara De Silva et al. “A Modular 1D-CNN Architecture for Real-time Digital Pre-distortion”. In: *2022 IEEE Topical Conference on RF/Microwave Power Amplifiers for Radio and Wireless Applications (PAWR)*. 2022, pp. 79–81. DOI: 10.1109/PAWR53092.2022.9719754.

[33] Diederik P. Kingma and Jimmy Ba. *Adam: A Method for Stochastic Optimization*. 2017. arXiv: 1412.6980 [cs.LG].

[34] D.R. Morgan et al. “A Generalized Memory Polynomial Model for Digital Predistortion of RF Power Amplifiers”. In: *IEEE Transactions on Signal Processing* 54.10 (2006), pp. 3852–3860. DOI: 10.1109/TSP.2006.879264.

A

Details of Performance Results for Doherty PA

SGRU				
NMSE (dB)	ACPR_L (dBc)	ACPR_R (dBc)	EVM (dB)	#params
N/A	-28.89	-30.5	-24.58	w/o DPD
-36.57±0.51	-43.88±0.13	-43.83±0.86	-37.33±0.40	150
-37.17±0.62	-44.31±0.21	-45.16±0.39	-37.72±0.15	394
-37.15±0.21	-44.35±0.22	-45.58±0.21	-37.77±0.14	552
-37.05±0.19	-44.43±0.20	-45.62±0.24	-37.80±0.17	1170
-36.94±0.08	-44.87±0.18	-45.79±0.33	-37.82±0.01	1702
-37.16±0.12	-44.89±0.32	-45.61±0.18	-37.84±0.10	2330

Table A.1: The test results of SGRU for 100 MHz OFDM signal on Doherty PA.

DVR-JANET				
NMSE (dB)	ACPR_L (dBc)	ACPR_R (dBc)	EVM (dB)	#params
-36.55±0.63	-42.53±0.79	-42.99±1.11	-37.05±0.59	145
-37.17±0.28	-43.22±1.00	-45.04±0.92	-37.70±0.26	397
-36.98±0.14	-43.36±0.34	-45.22±0.26	-37.71±0.14	509
-36.93±0.08	-43.62±0.33	-45.28±0.24	-37.91±0.15	1097
-36.96±0.09	-43.66±0.34	-45.59±0.13	-37.94±0.23	1909
-37.04±0.40	-44.16±0.48	-45.45±0.16	-37.96±0.16	2450

Table A.2: The test results of DVR-JANET for 100 MHz OFDM signal on Doherty PA.

PG-JANET				
NMSE (dB)	ACPR_L (dBc)	ACPR_R (dBc)	EVM (dB)	#params
-34.95±0.34	-40.36±0.48	-40.34±0.71	-35.62±0.46	154
-36.85±0.28	-42.74±1.00	-44.52±0.92	-37.62±0.26	415
-36.59±0.26	-43.20±0.95	-43.29±1.28	-37.43±0.29	530
-37.10±0.14	-43.09±0.41	-45.57±0.41	-37.99±0.10	1130
-37.23±0.10	-43.12±0.63	-45.99±0.08	-37.98±0.09	1727
-36.98±0.17	-43.36±0.24	-45.97±0.51	-37.91±0.05	2450

Table A.3: The test results of PG-JANET for 100 MHz OFDM signal on Doherty PA.

VDLSTM				
NMSE (dB)	ACPR_L (dBc)	ACPR_R (dBc)	EVM (dB)	#params
-37.38±0.23	-43.20±0.67	-45.77±0.24	-38.23±0.30	130
-37.33±0.14	-43.39±0.66	-45.97±0.25	-38.16±0.20	310
-37.75±0.17	-44.23±0.30	-46.02±0.40	-38.20±0.16	562
-37.87±0.19	-44.27±0.44	-46.40±0.34	-38.14±0.23	1142
-37.29±0.40	-44.19±0.75	-46.25±0.20	-37.81±0.17	1922
-37.01±0.71	-43.95±0.54	-46.11±0.26	-37.01±0.61	2290

Table A.4: The test results of VDLSTM for 100 MHz OFDM signal on Doherty PA.

SGRU				
NMSE (dB)	ACPR_L (dBc)	ACPR_R (dBc)	EVM (dB)	#params
-23.73	-28.89	-29.86	-21.28	w/o DPD
-23.55±0.26	-37.84±0.37	-41.43±0.31	-24.09±0.16	150
-23.61±0.32	-37.85±0.44	-41.55±0.13	-24.09±0.07	394
-23.72±0.19	-37.96±0.42	-41.82±0.29	-24.14±0.10	552
-23.74±0.07	-38.06±0.48	-41.82±0.14	-24.20±0.30	1170
-23.82±0.42	-38.18±0.34	-41.87±0.10	-24.23±0.02	1702
-23.91±0.04	-38.31±0.42	-41.95±0.24	-24.24±0.06	2330

Table A.5: The test results of SGRU for 200 MHz OFDM signal on Doherty PA.

DVR-JANET				
NMSE (dB)	ACPR_L (dBc)	ACPR_R (dBc)	EVM (dB)	#params
-23.10±0.19	-33.94±0.24	-39.07±1.21	-23.87±0.05	145
-23.25±0.16	-33.95±0.11	-39.47±0.23	-23.88±0.10	397
-23.64±0.07	-34.02±0.12	-39.70±0.26	-23.99±0.09	509
-23.89±0.05	-34.10±0.29	-39.83±0.19	-24.03±0.02	1097
-23.90±0.05	-34.16±0.23	-39.90±0.18	-24.06±0.03	1909
-23.92±0.02	-34.30±0.15	-39.93±0.20	-24.06±0.02	2450

Table A.6: The test results of DVR-JANET for 200 MHz OFDM signal on Doherty PA.

PG-JANET				
NMSE (dB)	ACPR_L (dBc)	ACPR_R (dBc)	EVM (dB)	#params
-23.14±0.51	-35.77±1.34	-38.22±1.84	-23.91±0.22	154
-23.79±0.28	-37.60±0.47	-40.88±0.27	-24.03±0.03	415
-23.81±0.14	-37.98±0.17	-41.57±0.32	-24.05±0.05	530
-23.89±0.05	-37.91±0.18	-41.77±0.27	-24.1±0.05	1130
-23.99±0.7	-38.16±0.63	-41.78±0.16	-24.11±0.08	1727
-23.99±0.04	-38.52±0.51	-41.86±0.17	-24.11±0.07	2450

Table A.7: The test results of PG-JANET for 200 MHz OFDM signal on Doherty PA.

VDLSTM				
NMSE (dB)	ACPR_L (dBc)	ACPR_R (dBc)	EVM (dB)	#params
-23.81±0.07	-38.16±0.25	-41.89±0.44	-24.11±0.07	130
-24.1±0.09	-38.33±0.30	-42.01±0.13	-24.21±0.05	310
-24.2±0.03	-38.48±0.49	-42.06±0.28	-24.29±0.05	562
-24.18±0.10	-38.52±0.51	-42.08±0.25	-24.32±0.30	1142
-24.19±0.05	-38.42±0.42	-42.06±0.27	-24.24±0.04	1922
-24.20±0.05	-38.24±0.3	-41.96±0.09	-24.18±0.05	2290

Table A.8: The test results of VDLSTM for 200 MHz OFDM signal on Doherty PA.